Single-cell analyses reveal SARS-CoV-2 interference with intrinsic immune response in the human gut

Sergio Triana[1,2], Camila Metz Zumaran[3], Carlos Ramirez[4], Carmon Kee[3,5], Patricio Doldan[3,5], Mohammed Shahraz[1], Daniel Schraivogel[6], Andreas R. Gschwind[7], Lars M. Steinmetz[6,7,8], Carl Herrmann[4], Theodore Alexandrov[1,9#], Steeve Boulant[3,5#], Megan L. Stanifer[10#]

1. Structural and Computational Biology Unit, European Molecular Biology Laboratory, Heidelberg, Germany
2. Collaboration for joint PhD degree between EMBL and Heidelberg University, Faculty of Biosciences, Germany
3. Department of Infectious Diseases, Virology, Heidelberg University, Germany
4. Health Data Science Unit, Medical Faculty University Heidelberg and BioQuant, Heidelberg, Germany
5. Research Group "Cellular Polarity and Viral Infection", German Cancer Research Center (DKFZ), Heidelberg, Germany
6. Genome Biology Unit, European Molecular Biology Laboratory, Heidelberg, Germany
7. Department of Genetics, Stanford University School of Medicine, Stanford, California 94305, USA
8. Stanford Genome Technology Center, Palo Alto, California 94304, USA
9. Skaggs School of Pharmacy and Pharmaceutical Sciences, University of California San Diego, La Jolla, California, USA
10. Department of Infectious Diseases, Molecular Virology, Heidelberg University, Germany

#Corresponding authors:

Megan L. Stanifer, PhD
Department of Infectious Disease
Molecular Virology
Heidelberg University
Im Neuenheimer Feld 344
69120 Heidelberg, Germany
Phone: +49 (0) 6221 56 7865
Email: m.stanifer@dkfz.de

Steeve Boulant, Ph.D
Department of Infectious Disease
Virology
Heidelberg University
Im Neuenheimer Feld 344
69120 Heidelberg, Germany
Phone: +49 (0) 6221 56 7865
Email: s.boulant@dkfz.de

Theodore Alexandrov, PhD
Structural and Computational Biology Unit,
European Molecular Biology Laboratory
Meyerhofstraße 1
69117 Heidelberg, Germany
Phone: +49 (0) 6221 387 8690
Email: theodore.alexandrov@embl.de

28   **Abstract**

29   **Objective** Exacerbated pro-inflammatory immune response contributes to COVID-19 pathology.
30   Despite the evidence about SARS-CoV-2 infecting the human gut, little is known about the
31   importance of the enteric phase of SARS-CoV-2 for the viral lifecycle and for the development of
32   COVID-19-associated pathologies. Similarly, it remains unknown whether the innate immune
33   response triggered in this organ to combat viral infection is similar or distinct compared to the one
34   triggered in other organs.
35   **Design** We exploited human ileum- and colon-derived organoids as a non-transformed culture
36   model supporting SARS-CoV-2 infection. We characterized the replication kinetics of SARS-CoV-
37   2 in intestinal epithelial cells and correlated the expression of the viral receptor ACE2 with
38   infection. We performed conventional and targeted single-cell transcriptomics and multiplex
39   single-molecule RNA fluorescence in situ hybridization and used IFN-reporter bioassays to
40   characterize the response of primary human intestinal epithelial cells to SARS-CoV-2 infection.
41   **Results** We identified a subpopulation of enterocytes as the prime target of SARS-CoV-2. We
42   found the lack of positive correlation between susceptibility to infection and the expression of
43   ACE2 and revealed that SARS-CoV-2 downregulates ACE2 expression upon infection. Infected
44   cells activated strong proinflammatory programs and produced interferon, while expression of
45   interferon-stimulated genes was limited to bystander cells due to SARS-CoV-2 suppressing the
46   autocrine action of interferon in infected cells.
47   **Conclusion** Our findings reveal that SARS-CoV-2 curtails the immune response in primary
48   human intestinal epithelial cells to promote its replication and spread and this highlights the gut
49   as a proinflammatory reservoir that should be considered to fully understand SARS-CoV-2
50   pathogenesis.
51

<u>Significance of the study</u>

What is already known about this subject?
- COVID-19 patients have gastrointestinal symptoms which likely correlates with SARS-CoV-2 infection of the intestinal epithelium
- SARS-CoV-2 replicates in human intestinal epithelial cells.
- Intestinal organoids are a good model to study SARS-CoV-2 infection of the gastrointestinal tract
- There is a limited interferon response in human lung epithelial cells upon SARS-CoV-2 infection.

What are the new findings?
- A specific subpopulation of enterocytes are the prime targets of SARS-CoV-2 infection of the human gut.
- There is a lack of correlation between ACE2 expression and susceptibility to SARS-CoV-2 infection. SARS-CoV-2 downregulates ACE2 expression upon infection.
- Human intestinal epithelium cells produce interferon upon SARS-CoV-2 infection.
- Interferon acts in a paracrine manner to induce interferon stimulated genes that control viral infection only in bystander cells.
- SARS-CoV-2 actively blocks interferon signaling in infected cells.

How might it impact on clinical practice in the foreseeable future?
- The absence of correlation between ACE2 levels and susceptibility suggest that medications influencing ACE2 levels (e.g. high blood pressure drugs) will not make patients more susceptible to SARS-CoV-2 infection.
- The restricted cell tropism and the distinct immune response mounted by the GI tract, suggests that specific cellular restriction/replication factors and organ specific intrinsic innate immune pathways can represent unique therapeutic targets to treat COVD-19 patients by considering which organ is most infected/impacted by SARS-CoV-2.
- The strong pro-inflammatory signal mounted by the intestinal epithelium can fuel the systemic inflammation observed in COVID-19 patients and is likely participating in the lung specific pathology.

3

86
87
88

Introduction

90 Coronavirus Disease 2019 (COVID-19) is caused by the severe acute respiratory syndrome
91 coronavirus 2 (SARS-CoV-2). This highly infectious zoonotic virus has caused a global pandemic
92 with almost 30,000,000 people infected worldwide as of September 2020. An exacerbated pro-
93 inflammatory immune response generated by the host has been proposed to be responsible for
94 the symptoms observed in patients [1–3]. Numerous studies have correlated the nature and
95 extent of the immune response with the severity of the disease [4–6]. While many countries have
96 succeeded in curtailing the first wave of infection, there is growing evidence that a second wave
97 of infection is expected to take place and has even already started in some countries. Therefore,
98 it is very urgent that we understand the virus-induced pathogenesis, in particular the immune
99 response generated by the host, to develop prophylactic therapeutics, antiviral approaches and
100 pharmacological strategies to control and revert the pathologies seen in patients.

101

102 SARS-CoV-2 is a member of the betacoronavirus genus, which initiates its lifecycle by exploiting
103 the cellular receptor angiotensin converting enzyme 2 (ACE2) to enter and infect host cells [7].
104 Virus entry relies not only on ACE2, but also on the cellular proteases furin and the
105 transmembrane serine protease 2 (TMPRSS2) that cleave and activate the SARS-CoV-2
106 envelope spike protein [8]. Following release of the genome into the cytosol, translation of the
107 positive strand RNA genome is initiated and viral proteins quickly induce the formation of cellular
108 membrane-derived compartments for virus replication and *de novo* assembly of virus particles.
109 The host cells execute several strategies to counteract viral replication. Cellular pathogen
110 recognition receptors (PRRs) sense viral molecular signatures or pathogen-associated molecular
111 patterns (PAMPs) and induce a signaling cascade leading to the induction of interferons (IFNs)
112 and pro-inflammatory molecules. IFNs represent the first line of defense against viral infection as
113 their autocrine and paracrine signaling leads to the production of hundreds of interferon-
114 stimulated genes (ISGs) known to exert broad antiviral functions [9].
115 SARS-CoV-2 infection is not limited to the respiratory tract and COVID-19 patients show systemic
116 manifestation of the disease in multiple organs [10,11]. For many of these organs, it is unclear
117 whether the pathology is a side effect of SARS-CoV-2 infection in the lung and its associated pro-
118 inflammatory response or whether it is due to a direct SARS-CoV-2 infection of the specific organ.
119 For the gastrointestinal (GI) tract, there is clear evidence of SARS-CoV-2 replication which is
120 associated with the release of viral genome into the feces [12–15]. Human intestinal organoids
121 have been established as a robust model to study SARS-CoV-2 infection and provided direct
122 evidence about primary human intestinal epithelial cells efficiently supporting SARS-CoV-2
123 replication [16–18]. Importantly, while SARS-CoV-2 infection in the lung is characterized by a
124 curtailed IFN response [19,20], the intrinsic immune response in intestinal epithelial cells is
125 characterized by the production of IFN and ISGs, with IFNs providing some protection to intestinal
126 epithelium cells against SARS-CoV-2 [17]. Studies in human intestinal organoids revealed that
127 only discrete cells are susceptible to SARS-CoV-2 infection and some evidence suggests that

128   these cells may be enterocytes [16]. However, the precise cell tropism of SARS-CoV-2 within the
129   colon and other parts of the gastrointestinal tract is yet to be fully characterized. Finally, despite
130   the driving role of inflammation in the pathologies observed in COVID-19 patients, we are still
131   lacking important molecular details concerning the inflammatory response generated by SARS-
132   CoV-2 infected cells and how the surrounding bystander cells will respond to it.
133
134   Here, we aim to address the outlined gaps by applying single-cell RNA-sequencing to human
135   ileum- and colon-derived organoids infected with SARS-CoV-2. Using differential gene
136   expression analysis and multiplex single-molecule RNA fluorescence *in situ* hybridization (FISH),
137   we investigated the cell type tropism of SARS-CoV-2 and its link to ACE2 expression levels. While
138   we could show that immature enterocytes represent the primary site of SARS-CoV-2 infection,
139   we did not observe correlation between infectivity and ACE2 expression. Interestingly, we could
140   observe that SARS-CoV-2 infection is associated with a downregulation of ACE2 expression.
141   Pathway analysis revealed that infected cells mount a strong pro-inflammatory response
142   characterized by the upregulation of both NFκB/TNF expression and the activity of their respective
143   pathways. On the contrary, bystander cells were characterized by an upregulation of the IFN-
144   mediated immune response as monitored by the increased production of ISGs. Importantly, using
145   a combination of multiplex single molecule RNA FISH and IFN-reporter bioassays we could show
146   that while IFN could act in a paracrine manner in bystander cells, IFN cannot act in an autocrine
147   manner in SARS-CoV-2 infected cells. Our findings demonstrate that SARS-CoV-2 has
148   developed strategies to impair IFN-mediated signaling in infected cells, and together with our
149   previous observations showing that IFN restricts SARS-CoV-2 replication in intestinal cells [17],
150   these results suggest that SARS-CoV-2 manipulates the cell intrinsic innate immune response to
151   promote its replication and spread.
152

Results

Single-cell RNA sequencing of SARS-CoV-2 infected colon and ileum organoids
155   A fraction of COVID-19 patients show enteric symptoms and it has been shown that SARS-CoV-
156   2 replicates in the intestinal tract of patients [13] and in human primary intestinal epithelial cells
157   [16–18,21]. To characterize SARS-CoV-2 interactions with primary human intestinal epithelial
158   cells (hIECs) and to ultimately address whether the enteric phase of SARS-CoV-2 contributes to
159   the observed cytokine profiles and systemic inflammation observed in COVID-19 patients, human
160   intestinal organoids were infected by SARS-CoV-2. To address whether organoids derived from
161   distinct parts of the intestinal tract display different susceptibility, colon- and ileum-derived
162   organoids were infected by SARS-CoV-2 and their response was monitored along the course of
163   infection. For both colon- and ileum-derived organoids, we could observe the presence of infected
164   cells as early as 4 hours post-infection (hpi) with the number of infected cells increasing within
165   the course of infection (Fig. S1A). This was corroborated with an increase in intracellular viral
166   RNA and the release of *de novo* infectious virus particles over time (Fig. S1B-C) thus
167   demonstrating efficient virus replication and spreading of infection in both colon and ileum
168   organoids. To characterize how hIECs respond to SARS-CoV-2 infection, we monitored the
169   production of type I IFN (IFNβ1) and type III IFNs (IFNλ1 and IFNλ2-3) over time. SARS-CoV-2
170   did not induce significant production of IFNβ1 in either ileum or colon organoids, except for a slight

171 upregulation of IFNβ1 expression in colon organoids at 24 hpi (Fig. S1D, left panels). On the
172 contrary, for IFNλ2-3, a strong upregulation was observed in both colon and ileum organoids upon
173 infection by SARS-CoV-2 (Fig. S1D, right panels). Interestingly, similar to IFNβ1, IFNλ1 was not
174 upregulated in response to infection (Fig. S1D, middle panels). Taken together, these results
175 show that a fraction (around 10%) of human intestinal epithelial cells fully supports SARS-CoV-2
176 infection, replication, *de novo* production of infectious virus particles and that infection is
177 associated with the upregulation of type III IFNs (IFNλ2-3) (Fig. S1A).
178
179 **Determination of SARS-CoV-2 intestinal epithelial cell tropism**
180 Human intestinal organoids are composed of multiple cell types recapitulating the cellular
181 complexity of the human intestinal epithelium. Although it is clear that SARS-CoV-2 infects the
182 human intestinal epithelium, which specific cell types are infected by the virus, how infection
183 impacts the transcriptional landscape of each individual cell type and how bystander cells respond
184 to viral infection remains unknown. To characterize SARS-CoV-2 interactions with hIECs at the
185 single-cell transcriptional level, colon- and ileum-derived organoids were infected with SARS-
186 CoV-2 and subjected to single-cell RNA sequencing (scRNAseq) (Fig. 1A). Single-cell
187 suspensions were generated and 3' scRNAseq was performed across six biological conditions
188 (mock, 12 hpi and 24 hpi for both colon and ileum organoids). scRNAseq provided broad
189 transcriptional profiles for around 2000 cells per condition with 5000 and 6000 genes profiled on
190 average per cell for the colon and the ileum, respectively (Fig. S2A-F for colon organoids and Fig.
191 S2G-L for ileum organoids).
192
193 To identify the cell types present in our organoids, we used the Uniform Manifold Approximation
194 and Projection (UMAP) algorithm for dimensionality reduction of our scRNAseq data. We
195 identified eight and nine clusters of cells in the colon and ileum organoids, respectively (Fig. 1B).
196 Using both cell-type-specific marker genes (Fig. 1C) from single-cell atlases of human intestinal
197 tissues [22]and our annotated scRNAseq data from human Ileum biopsies [23], we could identify
198 the cell types represented in these clusters (Fig. 1B). Stem cells, transient amplifying (TA) cells,
199 enterocytes, goblet and enteroendocrine cells were found to be present in intestinal organoids
200 (Fig. 1B). Different subpopulations of enterocytes in ileum and colon (CLCA4+, ALDOB+,
201 MUC13+), were identified, namely, enterocytes 1 (GUCA2A+, FABP6+, CA4+), enterocytes 2
202 (MMP7+,MUC1+, CXCL1+) as well as immature enterocytes 1 and immature enterocytes 2, the
203 latter likely representing cells not fully differentiated into mature enterocytes. The presence of two
204 distinct populations of enterocytes and their immature related forms is consistent with previous
205 reports [22]. Importantly, infection by SARS-CoV-2 did not alter cell clustering (Fig. 1B, left UMAP
206 inset panels) and did not impact the proportions of the different cell types present in both the colon
207 and ileum organoids (Fig. 1D) thus allowing us to investigate cell tropism.
208
209 To increase the sensitivity and dynamic range in detecting the SARS-CoV-2 genome and selected
210 host genes, we made use of additional targeted scRNA-seq (Schraivogel et al. 2020) performed
211 on the same organoid samples. Targeted scRNA-seq is more sensitive to detect genes-of-interest
212 irrespective of their expression level, and quantifies gene expression with a higher dynamic range
213 compared to conventional 3' scRNAseq [24]. We selected 12 genes, including the SARS-CoV-2
214 genome, the SARS-CoV-2 receptor ACE2, an interferon stimulated gene (ISG15) and a panel of

215 hIEC type markers that we previously determined by scRNAseq of ileum biopsies and organoids
216 (APOA4, CHGB, FABP6, FCGBP, LYZ, MKI67, OLFM4, SLC2A2, SMOC2 and SST) [23].
217 Looking at the relative expression of SARS-CoV-2 genome in mock vs infected cells (Fig. S3A-
218 B), classical 3' scRNAseq detected the viral genome in a proportion of organoid cells (Fig. S3A
219 (inset); ~75% at 12 hpi and ~25% at 24 hpi), while using the targeted approach, SARS-CoV-2
220 counts were detected in virtually all cells in the infected samples (Fig. S3B). Concurrently, we
221 observed that the number of SARS-CoV-2 counts per cell increased over the course of infection
222 both targeted and whole transcriptome scRNA-seq (Fig. S3A-B), consistent with active replication
223 of the virus in organoids monitored using q-RT-PCR (Fig. S1B). Since it is expected that only a
224 fraction of the cells present in intestinal organoids are indeed infected by SARS-CoV-2 (Fig. S1A)
225 [16,17], the presence of SARS-CoV-2 genome in all cells likely does not reflect active viral
226 replication, but could be explained by the presence of viruses attached to the cells surface or by
227 free-floating viral particles or RNA. Capitalizing on the high dynamic range provided by targeted
228 scRNA-seq, we defined cells having productive infection and replication as those with the SARS-
229 CoV-2 counts higher than a baseline, calculated as the mean expression of SARS-CoV-2
230 measured by targeted scRNA-seq in all cells-containing droplets (Fig. S3C-D, top panels). Cells
231 with targeted scRNA-seq SARS-CoV-2 expression levels below the estimated baseline level were
232 defined as non-infected bystander cells. Following this approach, we could correct for the
233 presence of contaminating viral RNA. Only a small fraction of cells (Colon: 4.5% and Ileum: 5.2%)
234 was detected as supporting SARS-CoV-2 infection (Fig. S3C-D, UMAP bottom panels) which is
235 consistent with our immunofluorescence staining of SARS-CoV-2 infected organoids (Fig. S1A)
236 and other reports [16,17].
237
238 Comparing the targeted scRNA-seq and the conventional 3' scRNAseq approaches, we observed
239 high correlation between the expression levels estimated by these technologies (Fig. S3E-F top
240 panels), with targeted scRNA-seq providing several orders of magnitude higher dynamic range,
241 compared to the conventional 3' scRNA-seq (Fig. S3E-F bottom panels). The high positive
242 correlation between the two sequencing approaches (except for SLCA2) serves as a quality
243 control confirming that targeted scRNAseq could robustly quantify both viral and cellular genes.
244
245 While SARS-CoV-2 could be detected in most cell types in both colon and ileum organoids (Fig.
246 2A), immature enterocytes 2 consistently represented the main virus-targeted cell type (Fig. 2B).
247 The proportion of infected immature enterocytes 2 and the number of SARS-CoV-2 genome copy
248 per cell increased over the course of infection (Fig. 2B) which is consistent with both the increasing
249 number of infected cells observed by immunofluorescence and the increasing copies of SARS-
250 CoV-2 genome over time (Fig. S1A-B, S3A-B). In ileum-derived organoids, TA cells in the
251 secretory lineage were also found to be highly infected by SARS-CoV-2 (Fig. 2B, right panel).
252 Interestingly, these cells were infected mostly at 24 hpi, suggesting that they are secondary
253 targets of infection. Taken together, these results suggest that immature enterocytes 2 are the
254 primary target of SARS-CoV-2 infection in hIECs both in colon and ileum.
255
256 **SARS-CoV-2 cell tropism and association with expression of ACE2 and TMPRSS2**
257 The angiotensin-converting enzyme 2 (ACE2) and the cellular protease type II transmembrane
258 serine protease 2 (TMPRSS2) are known to be major determinants for SARS-CoV-2 infection.

7

259   ACE2 is the cellular receptor of SARS-CoV-2 mediating viral entry [7]. TMPRSS2 is a cellular
260   protease that processes the SARS-CoV-2 spike (S) protein which is an essential step for viral
261   envelope fusion with the host membrane and release of viral contents in the cytosol of the cells.
262   Combined conventional and targeted scRNAseq enabled us to investigate the link between
263   SARS-CoV-2 genome copy numbers and expression of ACE2 in a cell type-specific manner.
264   Different to what we have expected, immature enterocytes 2, the main site of SARS-CoV-2
265   infection in both colon and ileum organoids (Fig. 2A-B), were not the cells displaying the highest
266   levels of ACE2 (Fig. S4A-B). Analysis of ACE2 expression levels in all cell types revealed that
267   cells with relatively high levels of ACE2 (*e.g.* enterocytes 1) were not susceptible to SARS-CoV-
268   2 infection (Fig. 2B-C). Similarly, we found that SARS-CoV-2 infection is not associated with the
269   expression of the receptor structural homologue ACE, a candidate receptor for SARS-CoV-2
270   basigin (BSG, also known as CD147), as well as the cellular proteases furin, Cathepsin L1
271   (CTSL), aminopeptidase ANPEP and DPP4 (MERS-CoV receptors) (Fig. 2C). On the contrary,
272   TMPRSS2 was found to be highly expressed in immature enterocytes 2 (Fig. 2C). In summary,
273   although ACE2 is a recognized receptor for SARS-CoV-2, we found no association between
274   ACE2 expression levels and susceptibility to infection on the single-cell level or across detected
275   types of hIECs.

276

277

278   **SARS-CoV-2 infection induces downregulation of ACE2 expression in intestinal organoids**
279   ACE2 has been reported to act as an interferon stimulated gene (ISG) resulting in an increased
280   expression level upon viral infection and interferon stimulation of nasal and lung epithelial cells
281   [25]. Similarly, in COVID-19 patients, ACE2 expression was shown to be upregulated in lung
282   epithelial cells compared to control patients [26]. To investigate whether the expression of either
283   ACE2 or other putative receptors and key cellular proteases is upregulated upon SARS-CoV-2
284   infection or upon SARS-CoV-2-mediated immune response in primary hIECs, we compared their
285   expression levels in mock-infected cells *vs.* both SARS-CoV-2-infected and non-infected
286   bystander cells. Although we did not observe any association between ACE2 expression in non-
287   infected cells and their propensity to be infected by SARS-CoV-2 (Fig. 2B-C and S4A-B),
288   differential gene expression analysis revealed that upon SARS-CoV-2 infection the ACE2
289   expression levels were downregulated (Fig. 3A-B). In colon organoids, visible downregulation of
290   ACE2 expression was observed in infected cells, progressing from 12 hpi to 24 hpi, as compared
291   to mock-infected cells (Fig. 3B, left panel). Importantly, no significant difference of ACE2
292   expression in the bystander cells was observed (Fig. 3B). In ileum-derived organoids, ACE2
293   expression was also downregulated in the infected cells. However, in contrast to colon organoids,
294   ACE2 expression in bystander cells of ileum organoids was also downregulated as compared to
295   mock-infected cells (Fig. 3B, right panels). Moreover, ACE2 expression was found to be
296   negatively correlated with the presence of the viral genome (Fig. 3C-D). The downregulation of
297   ACE2 expression was not only observed in immature enterocytes 2 which were identified as the
298   primary site of SARS-CoV-2 infection (Fig. 2B), but it was also observed in most other cell types
299   present in ileum-derived organoids over the course of SARS-CoV-2 infection (Fig. 3E).
300   Expression levels of the other SARS-CoV-2 putative receptors and of key cellular proteases (e.g.
301   TMPRSS2, furin and CTSL) were also found to be reduced in both infected and bystander cells
302   in ileum derived-organoids as compared to mock-infected cells (Fig. 3B, right panel). Interestingly,

303 when considering colon-derived organoids, the expression levels of these cellular genes were
304 found slightly increased at 12 hpi and decreased at 24 hpi (Fig. 3B, left panel). Altogether, these
305 data suggest that ACE2 expression is downregulated in colon- and ileum-derived hIECs upon
306 SARS-CoV-2 infection. To validate this observation, we performed multiplex single-molecule
307 fluorescence *in situ* hybridization (FISH) on SARS-CoV-2 infected organoids. At 12 and 24 hpi,
308 organoids were fixed and evaluated using transcript-specific probes directed against the SARS-
309 CoV-2 genome and ACE2. Fluorescence microscopy analysis confirmed that infected cells indeed
310 display lower expression levels of ACE2 at both 12 hpi and 24 hpi (Fig. 3F, white arrow).
311 Quantification of the relative expression levels of SARS-CoV-2 genome and ACE2 transcripts in
312 the RNA FISH images at the single-cell level again confirmed a negative correlation between
313 SARS-COV-2 and ACE2 (Fig. 3G). Altogether, our data strongly suggest that the expression
314 levels of ACE2 decrease in both colon and ileum hIECs upon SARS-CoV-2 infection.
315

316 **SARS-CoV-2 induces a pro-inflammatory response in hIECs**
317 To evaluate the response of hIECs to SARS-CoV-2 infection, we performed a comparative gene
318 expression analysis between mock-infected and infected organoids. For the infected organoids,
319 we considered separately the infected cells (those with SARS-CoV-2 genome detected) and the
320 bystander cells (those without SARS-CoV-2 genome). In colon organoids, already at 12 hpi hIECs
321 display a strong NFκB and TNF response to infection with this response becoming even more
322 pronounced at 24 hpi (Fig. S5A-B). When comparing mock to bystander cells, we noticed that at
323 24 hpi, the response of bystander cells mostly followed an IFN-mediated immune response
324 characterized by the presence of multiple ISGs (Fig. S5C-D). This observation suggests that
325 infected cells generate a pro-inflammatory response while bystander cells likely respond to the
326 secreted IFN in a paracrine manner. This is supported by the differential gene expression analysis
327 of bystander vs. infected cells showing that infected cells have a stronger NFκB and TNF
328 mediated response compared to bystander cells (Fig. S5E-F). Similar results were found in
329 SARS-CoV-2 infected ileum-derived organoids (Fig. S5G-L). Interestingly, at 24 hpi, some
330 interferon-stimulated genes (ISGs) (e.g. IFIT1-3, MX1, CXCL10, IRF1) were found to be also
331 upregulated in infected cells but to a much lesser extent compared to bystander cells (Fig. S5G-
332 J). Additionally, while infected cells in ileum-derived organoids were found to generate a similar
333 NFκB/TNF-mediated response compared to the colon-derived organoids (Fig. S5B and H), ileum-
334 derived bystander cells had a stronger IFN-mediated response which can be seen by the overall
335 higher expression of ISGs in ileum organoids compared to colon organoids upon SARS-CoV-2
336 infection (Fig. S5D and J). Together, these comparative gene expression analyses revealed that
337 upon SARS-CoV-2 infection of human intestinal epithelial cells, both strong pro-inflammatory and
338 IFN-mediated responses are generated.
339

340 **Cell type specific immune response in infected vs. bystander cells**
341 Taking into account the differences in the susceptibility of the different hIEC types to SARS-CoV-
342 2, with immature enterocytes 2 constituting the main site of SARS-CoV-2 infection (Fig. 2), we
343 compared the response of each individual cell type to SARS-CoV-2 infection. Similar to the
344 analysis of all cell types taken together (Fig. S5), differential gene expression analysis of colon-
345 derived infected immature enterocytes 2 revealed a strong NFκB/TNF-mediated response while
346 bystander immature enterocytes 2 mostly display an IFN-mediated response (Fig. 4A-C and Fig.

9

347   S6A). Similarly, in ileum-derived organoids, infected immature enterocytes 2 also showed a strong
348   NFκB/TNF-mediated response (Fig. 4F, 4H and S6B) while bystander cells were characterized
349   by their response to secreted IFNs leading to ISG expression (Fig. 4G and Fig. S6B)
350
351   Pathway analysis confirmed that the bystander response was mostly an IFN-related response
352   while the infected cell response was mostly pro-inflammatory (Fig. S7). Comparison of the
353   transcriptional response to SARS-CoV-2 infection in infected *vs.* bystander immature enterocytes
354   2 further confirmed that infected cells mount a strong pro-inflammatory response characterized
355   by the upregulation of NFκB and TNF (Fig. 4C-D and 4H-I). Analysis of the top 30 differentially
356   expressed ISGs in colon-derived organoids clearly shows that at 24 hpi, bystanders cells respond
357   to IFN by upregulating the expression of a large panel of ISGs (Fig. 4E). Similar findings were
358   observed in immature enterocytes 2 from ileum organoids, although infected cells were also found
359   to express more ISGs compared to their colon-derived counterparts. Importantly, in both colon
360   and ileum organoids, bystanders showed higher levels of expression for all considered ISGs
361   compared to infected cells (Fig. 4E and 4J). These results are consistent with the observation that
362   ileum-derived organoids are more immune-responsive compared to colon-derived organoids (Fig.
363   S5D and J). Together these data show that upon SARS-CoV-2 infection, infected cells mount a
364   strong NFκB/TNF-mediated pro-inflammatory response and display a limited production of ISGs
365   while bystander cells mount a strong IFN-mediated response through a strongly-upregulated
366   expression of a broad panel of ISGs.
367
368   To determine if the characterized NFκB/TNF-high and IFN-low immune response is specific to
369   immature enterocytes 2, we also looked individually at each infected cell type. We found that in
370   all considered types of hIECs, bystander cells display an IFN-mediated response during SARS-
371   CoV-2 infection while infected cells are characterized by a strong NFκB/TNF-mediated response
372   (Fig. S8-9). Since our targeted scRNAseq analysis revealed the presence of background viral
373   RNA in the samples (Fig. S3), we asked whether the observed immune response is indeed
374   cascading to bystander cells through type III interferon secreted by infected cells or is caused by
375   the direct action of non-replicating viral particles on bystander cells. To address this, colon and
376   ileum organoids were infected with either live or UV-inactivated SARS-CoV-2. Results revealed
377   that upon infection with live SARS-CoV-2 both IFNs and ISGs were produced (Fig. S10). On the
378   contrary, exposure of organoids to UV-inactivated SARS-CoV-2 did not lead to virus replication
379   and cells failed to produce both IFN and ISGs (Fig. S10). This demonstrates that active replication
380   is required for the described immune response and allowed us to rule out the exposure to non-
381   replicating viral particles as being the cause of this response. Altogether our results show that
382   infected and bystander cells respond differently to SARS-CoV-2 infection where infected cells
383   mount a NFκB/TNF-mediated response while bystander cells mount a IFN-mediated response.
384

385   **Signaling activity in infected vs. bystander cells**
386   To characterize the signaling that underpins the distinct immune response of infected and
387   bystander cells upon SARS-CoV-2 infection, we inferred the pathway signaling activity from
388   scRNAseq data with PROGENy (Fig. 5A-B). For both colon and ileum organoids, infected cells
389   show a strong activation of the MAPKs, NFκB and TNFα pathways. In line with the enrichment
390   analysis (Fig. S7, S8), these pathways were found to be less activated in bystander cells with

391   higher scores in ileum compared to colon (Fig. 5A-B). Interestingly and in accordance with our
392   differential gene expression analyses (Fig. 4, S5 and S6), the JAK-STAT signalling pathway was
393   found to be activated mostly in bystander cells (Fig. 5A-B). To further elucidate the signalling
394   activity at the single-cell level, we generated diffusion maps of all single cells based on the
395   scRNAseq expression of interferon-related genes (Fig. 5C-D). In both iluem and colon, we
396   observed a clear bifurcation of all cells into two distinct branches, one branch representing mainly
397   infected cells and another branch representing mainly bystander cells. In addition, we calculated
398   the activities of selected transcription factors (TFs) for all single cells using SCENIC and mapped
399   the inferred activities onto the single-cell diffusion maps (Fig. 5C-D, right insets). We found that
400   the transcription factors STAT1 and IRF1 were activated mainly in bystander cells (branch along
401   DC1) while JUN was activated in infected cells (branch along DC2) (Fig. 5C-D, left panels).
402   Extending this analysis to transcription factors whose activity pattern is highly correlated to either
403   DC1 or DC2 revealed that globally, transcription factors that are critical for IFN-mediated signaling
404   (i.e. the ISGF3 complex: STAT1/STAT2/IRF9 and IRF1) are highly active in bystander cells (Fig.
405   5E-F). Similarly, the ETS variant transcription factor 7 (ETV7) which is an ISG acting as a negative
406   regulator of IFN-mediated signaling [27] and the Early Growth Response Gene 1 (EGR1) which
407   enhances type I IFN signalling [28] were also found to be activated in bystander cells (Fig. 5E-F).
408   Upregulation of the EGR1 and JUN dependent pathways was consistent with the findings of the
409   previous work investigating SARS-CoV-2 infection of the human lung and intestinal epithelial cell
410   lines Calu-3 and Caco-2 [29].
411

412   **SARS-CoV-2 inhibits IFN-mediated ISG expression**
413   To validate that the IFN-mediated response is specific to bystander cells, ileum-derived organoids
414   were infected with SARS-CoV-2. At 12 and 24 hpi, single molecule RNA FISH was performed
415   using probes specific for the SARS-CoV-2 genome and for ISG15 which was found to be highly
416   upregulated upon infection and has the highest -log10 *p*-value in the differential analysis
417   comparing bystander cells vs mock-infected cells (Fig. 4G). Microscopy images revealed that
418   bystander cells (non-infected) were indeed positive for ISG15 (Fig. 6A). Interestingly, SARS-CoV-
419   2 infected cells were found to express little to no ISG15 (Fig 6A, white arrows). Quantification
420   confirmed that cells which displayed the highest expression of ISG15 were negative for SARS-
421   CoV-2 genome (Fig. 6B). These results support the model that bystander cells respond to SARS-
422   CoV-2 infection by mounting an IFN-mediated response. On the other hand, as shown by using
423   both scRNAseq (Fig. 4) and RNA FISH (Fig. 6A), infected cells do not mount an IFN-mediated
424   response (low-to-no expression of ISGs) suggesting that infected cells are refractory to IFN. To
425   address whether SARS-CoV-2 infection can indeed impair IFN-mediated signaling, we directly
426   monitored ISG production in response to IFN treatment in either infected or non-infected cells.
427   However, while it is well known that ISGs are made in a JAK-STAT dependent manner
428   downstream the IFN receptors, there is growing evidence that a subset of ISGs can be made
429   downstream IRF3 following viral recognition by PRRs. To alleviate this unwanted IRF3 mediated
430   production of ISGs, we generated a human intestinal cell line (T84) depleted of IRF3. Infection of
431   the IRF3 KO T84 did not result in the production of ISGs as monitored by q-RT-PCR of ISG15
432   (Fig. 6D). IRF3 KO T84 cells were mock infected or infected with SARS-CoV-2, at 24 hpi cells
433   were treated with IFN and 12 h post-treatment production of ISG15 was assessed by q-RT-PCR
434   (Fig. 6C). Results show that mock infected IRF3 KO T84 cells were responsive to IFN

435 demonstrating that genetic depletion of IRF3 does not alter IFN-mediated signaling (Fig. 6D).
436 Interestingly, in SARS-CoV-2 infected IRF3 KO T84 cells, production of ISG15 upon IFN
437 treatment was significantly downregulated (Fig. 6D). To confirm that this impaired induction of
438 ISG15 upon IFN treatment was specific to SARS-CoV-2 infection, IRF3 KO T84 cells were
439 infected with astrovirus at an MOI of 3 to achieve full infection (Fig. 6E). Contrary to SARS-CoV-
440 2 infection, infection of IRF3 KO T84 cells by astrovirus did not impair IFN-mediated signaling as
441 a similar upregulation of ISG15 was observed in both mock-infected and astrovirus-infected cells
442 upon IFN treatment (Fig. 6D). In a second validation approach, to fully demonstrate that only
443 infected cells have an altered IFN-mediated signaling, we developed an assay based on a
444 fluorescent reporter of ISG expression (Fig. 6F). For this, we generated a T84 cell line transduced
445 with a reporter made of the promoter region of the ISG MX1 driving the expression of the
446 fluorescent protein mCherry. Mx1 is known to be made strictly downstream of the IFN receptor in
447 a JAK-STAT dependent manner but not downstream of IRF3. Upon IFN treatment, about 30-40%
448 of cells expressing this reporter were responsive and became fluorescent (Fig. 6G). Following
449 infection with SARS-CoV-2 at an multiplicity of infection (MOI) of 3, most of the cells were found
450 to be infected (Fig. 6G). However when cells were treated 24 hpi with IFN, most infected cells did
451 not respond to IFN and very few became double positive for both virus and MX1 driven mCherry
452 (Fig. 6G, left panel). To control that non-infected bystander cells could indeed respond to IFN and
453 express mCherry, we repeated this experiment but using an MOI of 1 for SARS-CoV-2 infection.
454 About 40% of the cells were found to be infected. Supplementing IFN affected mainly non-infected
455 cells, as can be seen from the increase of MX1-positive cells and no change in the number of
456 double-positive cells (both infected and MX1-positive) (Fig. 6G, right panel).
457
458 Altogether, our results provide a strong evidence that upon infection with SARS-CoV-2 primary
459 human intestinal cells generate a strong NFκB/TNF-mediated response and produce IFN. This
460 IFN acts in a paracrine manner onto bystander cells that leads to the upregulation of IFN-
461 stimulated genes. Importantly, SARS-CoV-2 infection renders infected cells refractory to IFN as
462 they show little-to-no increase in the activity of the JAK-STAT signaling pathways and fail to
463 upregulate IFN-stimulated gene expression.
464

465 **Discussion**

466 Many COVID-19 patients display gastroenteritis symptoms and there is growing evidence that the
467 intestinal epithelium can be infected by SARS-CoV-2. Whether the symptoms are associated with
468 the direct replication of SARS-CoV-2 in the GI tract or are a consequence of the strong pro-
469 inflammatory response seen in patients is unclear. Using human intestinal "mini-gut" organoids
470 has already demonstrated that intestinal epithelium cells can support SARS-CoV-2 infection,
471 replication and spread. However, which cell type is infected remains poorly defined [16–18]. By
472 exploiting single-cell transcriptomics approaches (scRNAseq) and targeted scRNAseq, we
473 identified that a subpopulation of enterocytes (namely, immature enterocytes 2) is the cell type
474 most susceptible to SARS-CoV-2 infection. Interestingly, other cell types also supported infection
475 by SARS-CoV-2 but to a much lesser extent (Fig. 2B). The characterized tropism of SARS-CoV-
476 2 could be explained by either cell type-specific intrinsic differences rendering some cell type
477 more permissive or due to an overrepresentation of cells of a particular cell type. In our colon-

478   derived organoids, there were twice as many immature enterocytes 1 compared to immature
479   enterocytes 2 and in ileum-derived organoids both enterocytes lineages were present in roughly
480   equal numbers. This suggests that the SARS-CoV-2 cell tropism for immature enterocytes 2 is
481   not due to a higher proportion of these cells in our organoids but due to intrinsic differences
482   between immature enterocytes 2 and other epithelial cell lineages. Differential gene expression
483   analysis between immature enterocytes 2 and the most similar other annotated cell type
484   (immature enterocytes 1) does not highlight the presence or absence of obvious
485   restriction/replication factors that could explain the observed tropism.
486

487   The expression levels of the SARS-CoV-2 receptor ACE2 were found to be higher in immature
488   enterocytes 1 while immature enterocytes 2 express more of the key cellular protease TMPRSS2
489   (Fig. 2C and S4). Although expression of ACE2 is mandatory for infection [7], we noticed no
490   correlation between ACE2 expression level and the copy numbers of SARS-CoV-2 genome in
491   the cell (Fig. 2B-C)(Fig. S11). This observation is important as it raises a question about using
492   ACE2 expression as the only basis for conjectures about infectability of cell types or even organs,
493   the approach recently proposed in various SARS-CoV-2-related publications [30–37]. Our results
494   highlight that the investigation of SARS-CoV-2 tropism requires biological validation of infection
495   and should not be done solely based on analysis of transcriptional profiles of individual cells or
496   tissues. Interestingly, we found that TMPRSS2 expression levels were well-associated with the
497   SARS-CoV-2 genome copy numbers in human intestinal epithelial cells (Fig. 2C and S4) which
498   is consistent with the observation that TMPRSS2 and the related protease TMPRSS4 are critical
499   for infection of intestinal organoids [18]. As such it is tempting to speculate that TMPRSS2 plays
500   a more important role in the SARS-CoV-2 cell tropism than ACE2, however more studies are
501   required to fully explore this hypothesis.
502

503   Several studies have suggested that ACE2 is an interferon-stimulated gene and is induced upon
504   SARS-CoV-2 infection [25,26]. This led to a speculation that upon infection and induction of pro-
505   inflammatory responses, the ACE2 levels would increase thereby favoring SARS-CoV-2 infection.
506   Our results show that, on the contrary, upon infection ACE2 levels decrease both in infected and
507   bystander hIECs (Fig. 3)(Fig. S11). Interestingly, differences in the kinetics of ACE2 regulation
508   were observed between colon- and ileum-derived organoids. In colon-derived organoids, a small
509   increase in ACE2 expression was observed at early times post-infection (12 hpi) but at later time
510   points (24 hpi) the overall expression of ACE2 (and other putative SARS-CoV-2 receptors and
511   key cellular proteases) was decreased as compared to mock infected cells (Fig. 3B). In ileum
512   organoids the expression of ACE2 was decreased over the time course of infection. The observed
513   upregulation of ACE2 upon infection might be tissue-specific and time-dependent. However,
514   recently it has been proposed that ACE2 does not behave as an ISG but instead a novel form of
515   ACE2 (dACE2) is interferon-inducible [38]. dACE2 results from transcription initiation at an
516   internal exon leading to the production of an alternative short version. Within our scRNAseq data
517   we could not distinguish between the two forms and as such the observed temporal increase (in
518   colon-derived organoids) could be due to the downregulation of ACE2 with the concomitant
519   upregulation of dACE2.
520

521   The nature of the PRR responsible for sensing SARS-CoV-2 infection is yet to be determined but
522   from recent work and previous work on SARS-CoV-1 and MERS it could be speculated that TLR3,
523   RLRs and the STING pathways could be involved [39,40]. In our current work we could show that
524   active virus replication is required to induce an IFN-mediated response as infection by UV-
525   inactivated SARS-CoV-2 did not lead to IFN and ISG production (Fig. S10). Interestingly, when
526   human intestinal epithelial cells are infected by a UV-inactivated reovirus, which is a virus whose
527   genome is a dsRNA, an IFN-mediated response is induced [41]. As SARS-CoV-2 is single-
528   stranded RNA virus and dsRNA intermediates will only occur during active replication, it is
529   tempting to speculate that what is being sensed are these dsRNA replication intermediates.
530

531   SARS-CoV-2 infection is characterized by a strong pro-inflammatory response and this has been
532   observed both in tissue-derived samples and *in vitro* using cell culture models [19]. This pro-
533   inflammatory response is characterized by upregulation of the NFκB and TNF pathways. Our
534   scRNAseq approach revealed that this pro-inflammatory response is specific to infected cells and
535   that bystander cells do not show a strong pro-inflammatory response. These differences between
536   infected and bystander cells were earlier observed for other cell types: infection of human
537   bronchial epithelial cells (HBECs) also reveal that the pro-inflammatory response is biased toward
538   infected cells and not bystander cells [31].
539

540   It was reported that infection of human lung epithelial cells by SARS-CoV-2 is characterized by a
541   low to absent IFN response [19]. On the contrary, in human intestinal epithelium cells an IFN-
542   mediated response is readily detectable and is characterized by both the production of IFN and
543   ISGs [16,17]. Interestingly, upon infection with SARS-CoV-2, we observed the upregulation of
544   IFNλ2-3 but we failed to observe a significant increase in IFNλ1 expression (Fig. S1D). This
545   absence of IFNλ1 upregulation is not specific to SARS-CoV-2 but a particularity of intestinal
546   organoids, as a similar IFNλ2-3 specific response was observed when intestinal organoids were
547   infected with other enteric viruses [42,43]. Upregulation of IFN production upon SARS-CoV-2
548   infection of intestinal epithelial cells was found to be low but significant (Fig. 4) and this could
549   raise the question whether this small production of IFN is sufficient to induce the production of
550   ISGs in a paracrine manner. Previous work on the antiviral function in type III IFN in human
551   intestinal epithelial cells revealed that although type III IFN protects epithelial cells against
552   infection in a dose-dependent manner, very small amounts of IFN are required to induce ISGs
553   and to provide an antiviral state to the cells [42]. The current work confirms this model as despite
554   a moderated upregulation of IFN expression in infected cells, we observed a strong ISG
555   upregulation in bystander cells.
556

557   When comparing the immune response generated by organoids derived from different sections
558   of the GI tract, we observed that ileum organoids were more immunoresponsive compared to
559   colon organoids. While the extent of the up-regulation of genes related to pro-inflammatory
560   response was similar between colon and ileum (Fig. 4A, 4F), we observed that ileum organoids,
561   particularly bystander cells produced significantly more ISGs compared to their colon counterparts
562   (Fig. 4b, 4G). This compartmentalization of response along the GI tract is consistent with previous
563   reports describing that different sections of the GI tract respond differently to microbial challenges
564   [44]. Most importantly, our results reveal that production of ISGs is mostly restricted to bystander

cells, while production of IFN is detected mostly in infected cells (Fig. 5, S5 and S6). These observed differences between infected and bystander cells were confirmed using single-molecule RNA FISH showing that production of ISG15 was clearly observed in bystander and, to a much lesser extent, in infected cells (Fig. 6). An important finding of this work is that infected cells not only fail to produce ISGs, they also become refractory to IFN (Fig. 6) (Fig. S11). When SARS-CoV-2-infected intestinal cells were treated with IFN, only bystander cells upregulated ISG while infected cells did not. This absence of ISG induction in infected cells suggests that SARS-CoV-2 has developed mechanisms to shutdown IFN-mediated signaling and the subsequent production of ISGs (Fig. S11). Preventing IFN-mediated signaling in infected cells would provide a replication advantage to SARS-CoV-2 as secreted IFN will not be able to act in an autocrine manner to induce ISGs which will curtail virus replication and *de novo* virus production. Although the SARS-CoV-2 viral protein responsible for blocking the IFN-mediated signaling is yet to be identified in our system, a recent report suggests that ORF6 could block IFN-mediated signaling by interfering with STAT1 nuclear translocation [45].

In conclusion, in this work we identified a subset of immature enterocytes as the primary site of infection of SARS-CoV-2 in ileum- and colon-derived human intestinal epithelial cells. We could show that upon infection, infected cells mount a strong pro-inflammatory response characterized by a strong activation of the NFκB/TNF pathways while bystander cells mount an IFN-mediated response (Fig. S11). This differential response between infected and bystander cells is due to an active block of IFN-signaling in infected cells (Fig. S11). Interestingly, recent work performing scRNAseq of SARS-CoV-2 infected HBECs revealed that infected cells were readily responding to secreted interferon and produced large amounts of ISGs [31]. This suggests that there are cell type-specific or tissue-specific regulations of interferon-mediated signaling during SARS-CoV-2 infection. This needs to be considered when studying replication and pathogenesis of SARS-CoV-2 in different organs as well as when developing therapies against COVID-19.

Acknowledgments

Author Contributions

ST performed experiments, analyzed the single cell data and contributed to manuscript writing. CR analyzed the single cell data. CMZ, CK, PD, MS and MLS performed experiments. DS and ARG performed target scRNA0seq. LS and CH contributed to the concept of the study and critical discussions. SB, MLS and TA conceived experiments, interpreted results and wrote the manuscript. The final version of the manuscript was approved by all authors.

Declaration of Interests

609   The authors declare no competing interests.
610
611
612
613
614
615
616
617
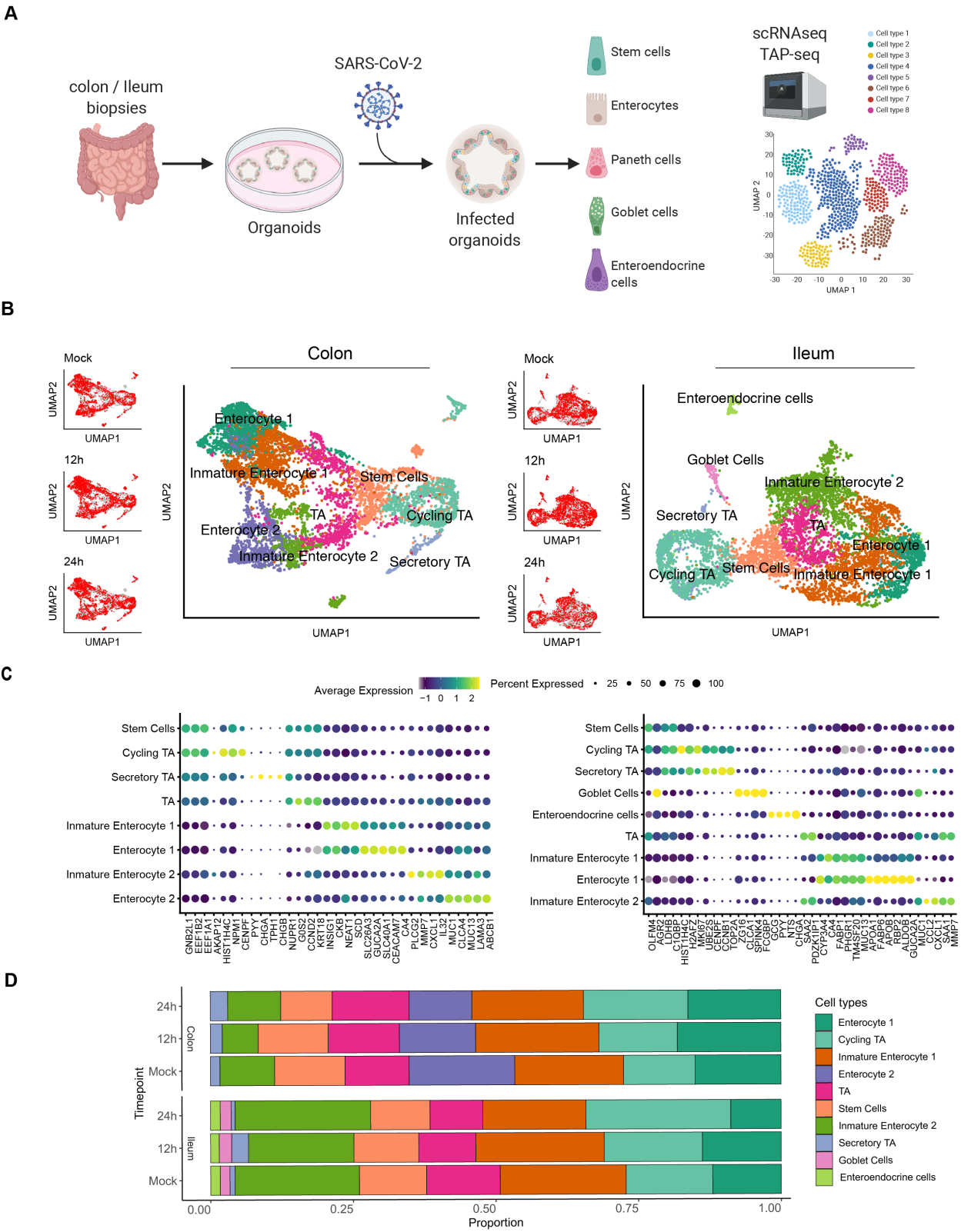618
619
620
621
622

623
624 **Figure 1.** Single cell sequencing of SARS-CoV-2 infected colon- and ileum-derived human

625 organoids. A. Schematic representation of the experimental workflow. B. Uniform manifold
626 approximation and projection (UMAP) embedding of single-cell RNA-Seq data from mock and
627 SARS-CoV-2 infected colon-derived (left panels) and ileum-derived (right panels) organoids
628 colored according to the cell type. Small insets represent the UMAP for mock and infected
629 organoids at 12 and 24 hpi. C. Dot plot of the top marker genes for each cell type for (left) colon-
630 and (right) ileum-derived organoids. The dot size represents the percentage of cells expressing
631 the gene; the color represents the average expression across the cell type. D. Bar plot displaying
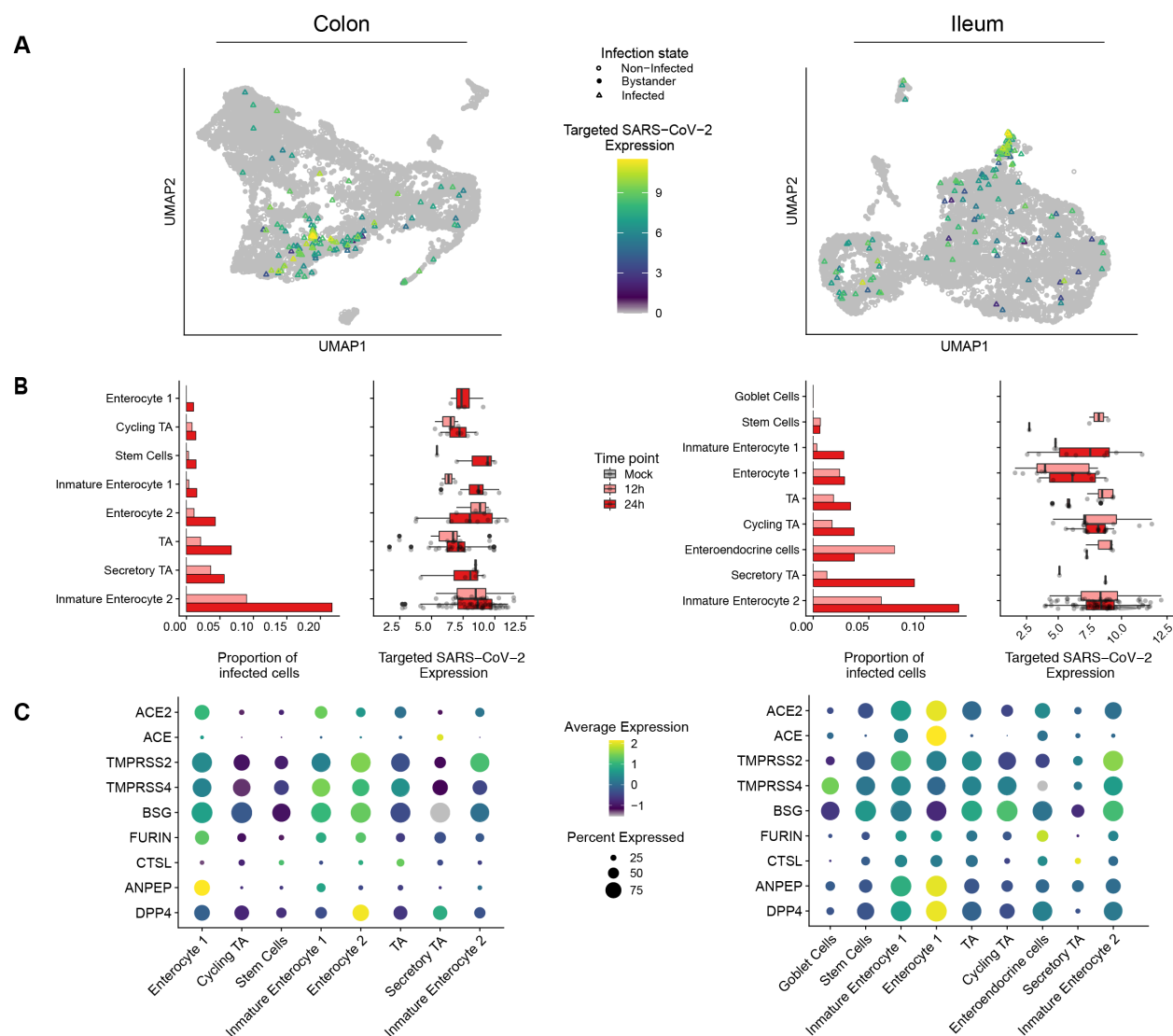632 the proportion of each cell type in mock and infected organoids (12 and 24 hpi).
633

Figure 2. SARS-CoV-2 cell tropism in human colon- and ileum-derived organoids. A. UMAP visualization of scRNAseq data of SARS-CoV-2 infected colon- (left) and ileum-derived organoids (right). Triangles represent infected cells and colors represent the corrected targeted normalized expression of SARS-CoV-2 determined using the targeted scRNAseq data. B. Proportion of cells infected with SARS-CoV-2 for each cell type and corresponding normalized expression values of SARS-CoV-2 in each individual cell type in colon (left) and ileum (right) organoids. Data are color coded for mock, 12 and 24 hpi. C. Dot plots of known entry determinants across cell types. The dot size represents the percentage of cells expressing the gene; the color represents the average expression across the cell type. Data are from mock-infected colon (left) and ileum organoids (right).
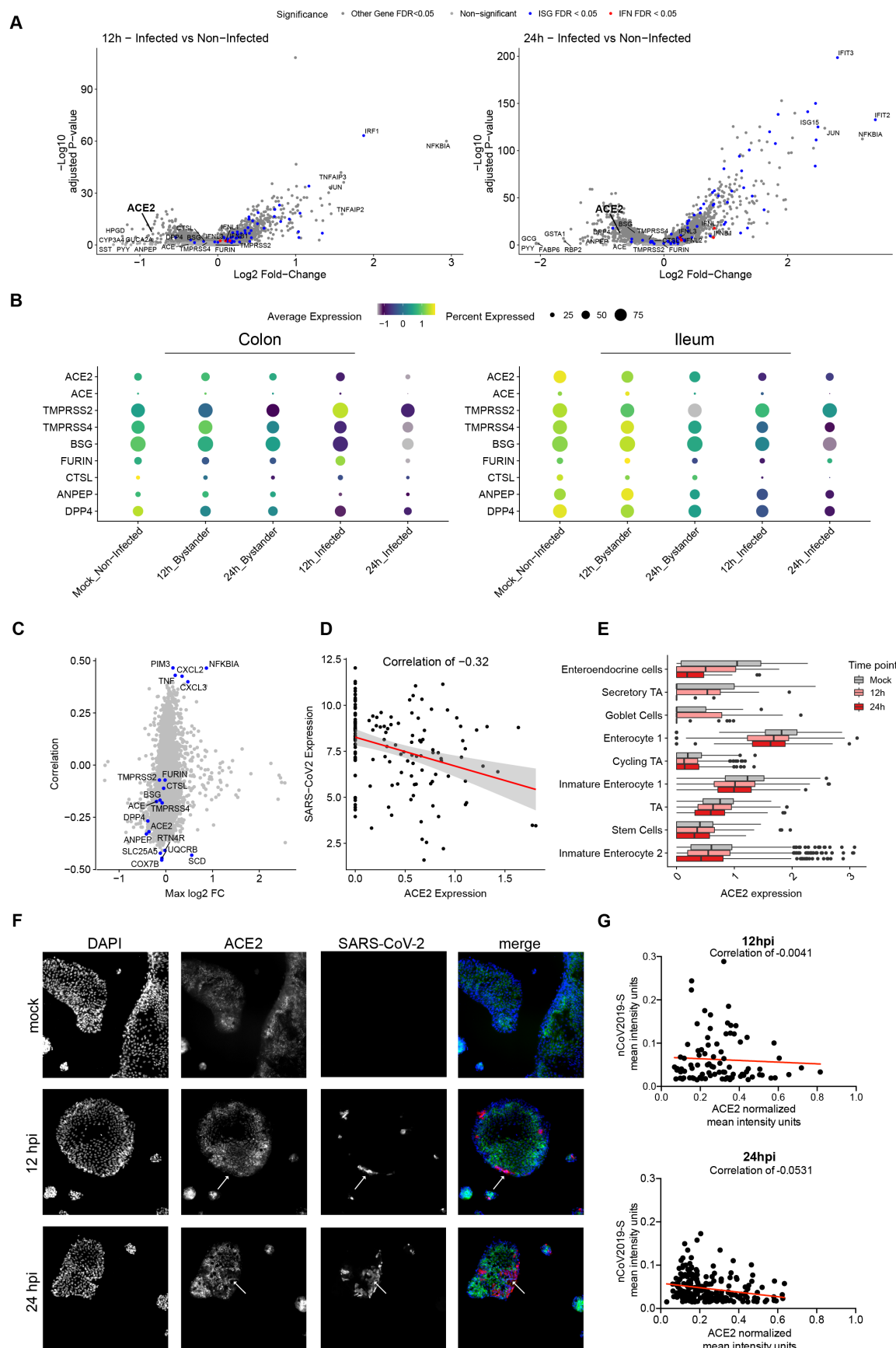
646

647 **Figure 3.** Downregulation of ACE2 upon SARS-CoV-2 infection. A. Volcano plots of genes that
648 are differentially expressed in infected cells relative to mock-infected cells at 12 hpi and 24 hpi in
649 ileum organoids. The statistical significance (-log10 of the adjusted p-value) is shown as a function
650 of the log2 fold change. B. Dot plots displaying the expression changes of known SARS-CoV-2
651 entry determinants for both infected and bystander cells during the course of infection (mock, 12
652 and 24 hpi) in colon (left) and ileum organoids (right). The dot size represents the percentage of
653 cells expressing the gene; the color represents the average expression across the cell type
654 excluding zeros. C. Correlation of gene expression values with the amount of SARS-CoV-2
655 genome (y-axis) vs the maximal log2 fold change (x-axis) across conditions. This plot is generated
656 by comparing both 12 and 24 hpi to mock. D. Correlation of SARS-CoV-2 expression with ACE2
657 expression across all cell types at 24 hpi. E. Expression values of ACE2 in each cell type for mock
658 infected and SARS-CoV-2 infected cells in ileum organoids at 12 hpi and 24 hpi. F. Multiplex in
659 situ RNA hybridization of ACE2 and SARS-CoV-2 of mock-infected and infected 2D ileum
660 organoids at 12 hpi and 24 hpi. White arrows point at SARS-CoV-2-infected cells. Representative
661 image is shown. G. Correlation of the relative expression SARS-CoV-2 and ACE2 for infected
662 cells from the multiplex in situ RNA hybridization shown in F. Each dot represents a cell.
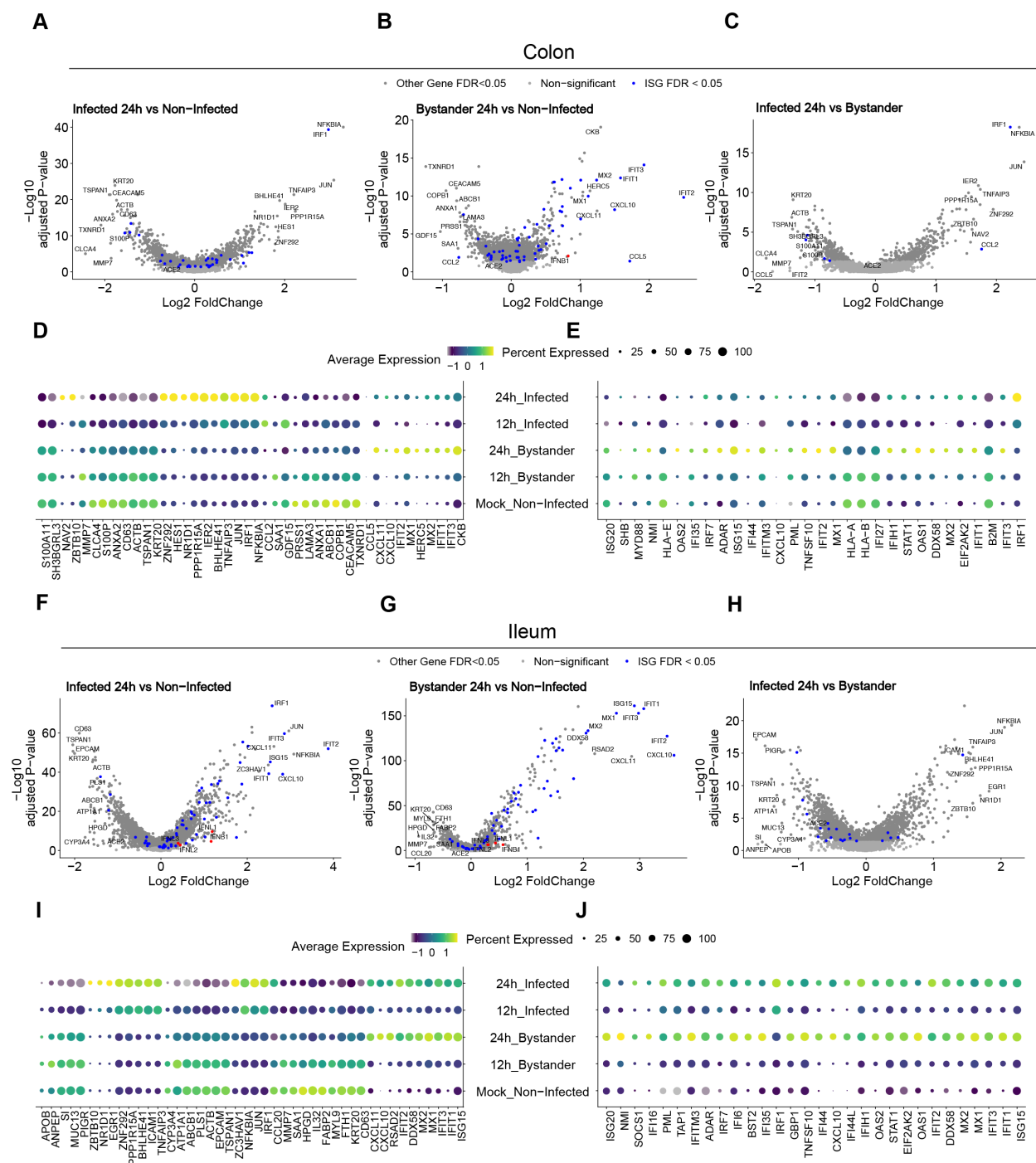663

664

Figure 4. Intrinsic innate immune response generated by immature enterocytes 2 upon SARS-CoV-2 infection. (A-C) Volcano plots displaying the genes that are differentially expressed in immature enterocytes 2 upon SARS-CoV-2 infection of colon organoids. A. infected vs. mock infected cells, B. bystander vs. mock infected cells and C. infected vs. bystander cells. The statistical significance (-log10 adjusted p-value) is shown as a function of the log2 fold change. D. Dot plot of the top 42 most differentially expressed genes upon SARS-CoV-2 infection in mock, infected and bystander cells at 12 and 24 hpi. The dot size represents the percentage of cells

22

672   expressing the gene; the color represents the average expression across the cell type. E. Same

673   as in D but for the top 30 most differentially expressed ISGs. F-G. Same as A-E but for ileum
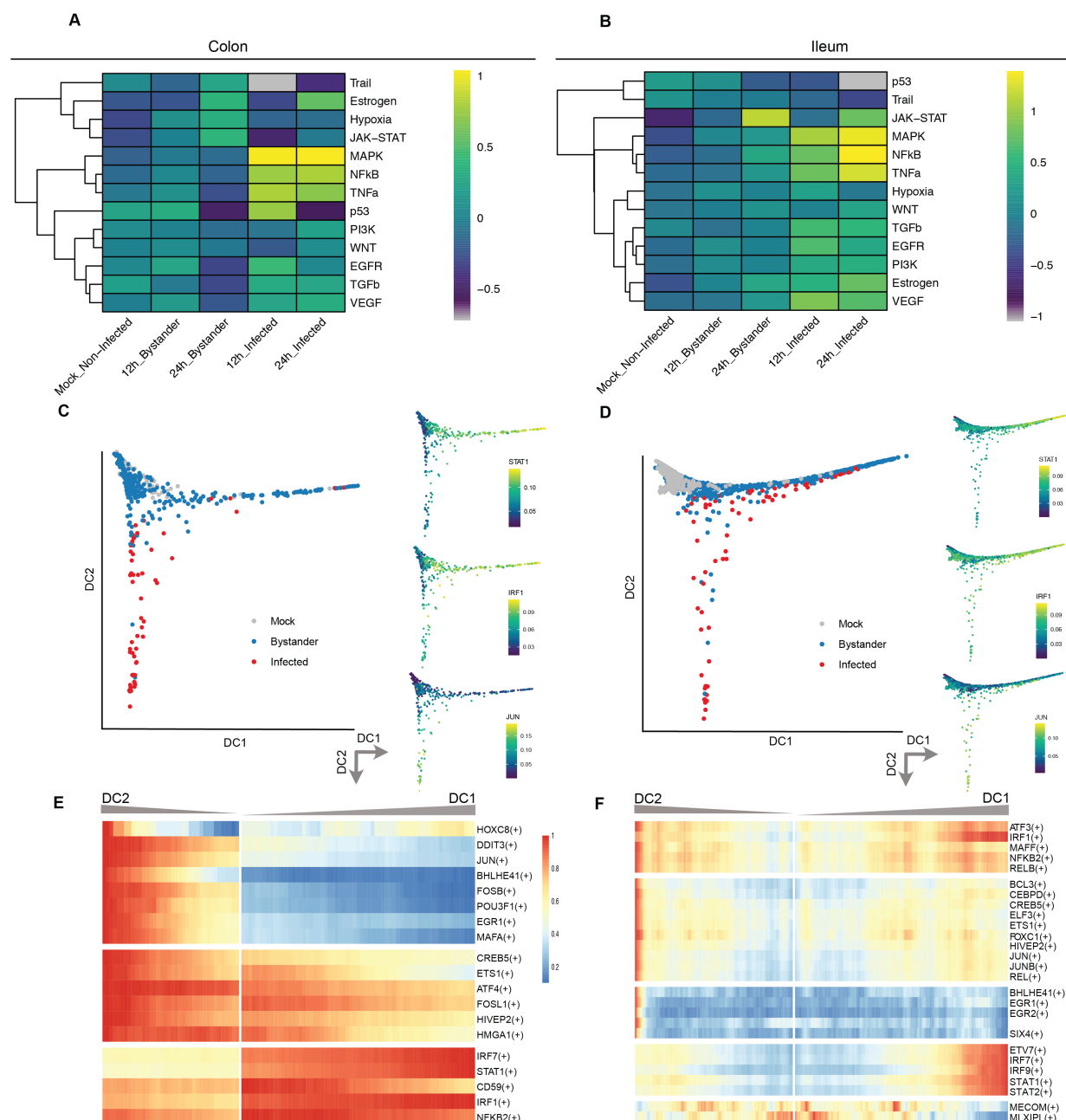
674   organoids.

675

Figure 5. Differential signaling activity of infected vs. bystander cells upon SARS-CoV-2 infection. A-B. Heatmaps of pathway signaling activity inferred by PROGENy for A. colon and B. ileum organoids. C-D. Diffusion maps embeddings showing mock, bystander and infected cells (big panels) and activities for selected transcription factors STAT1, IRF1 and JUN (small panels) for C. colon and D. ileum organoids. E-F. Heatmaps of transcription factor activities along bifurcating trajectories of the corresponding diffusion maps for E. colon and F. ileum organoids. The dimensions DC1 and DC2 represent the first two eigenvectors of the Markovian transition matrix and were calculated separately for either colon or ileum organoids.
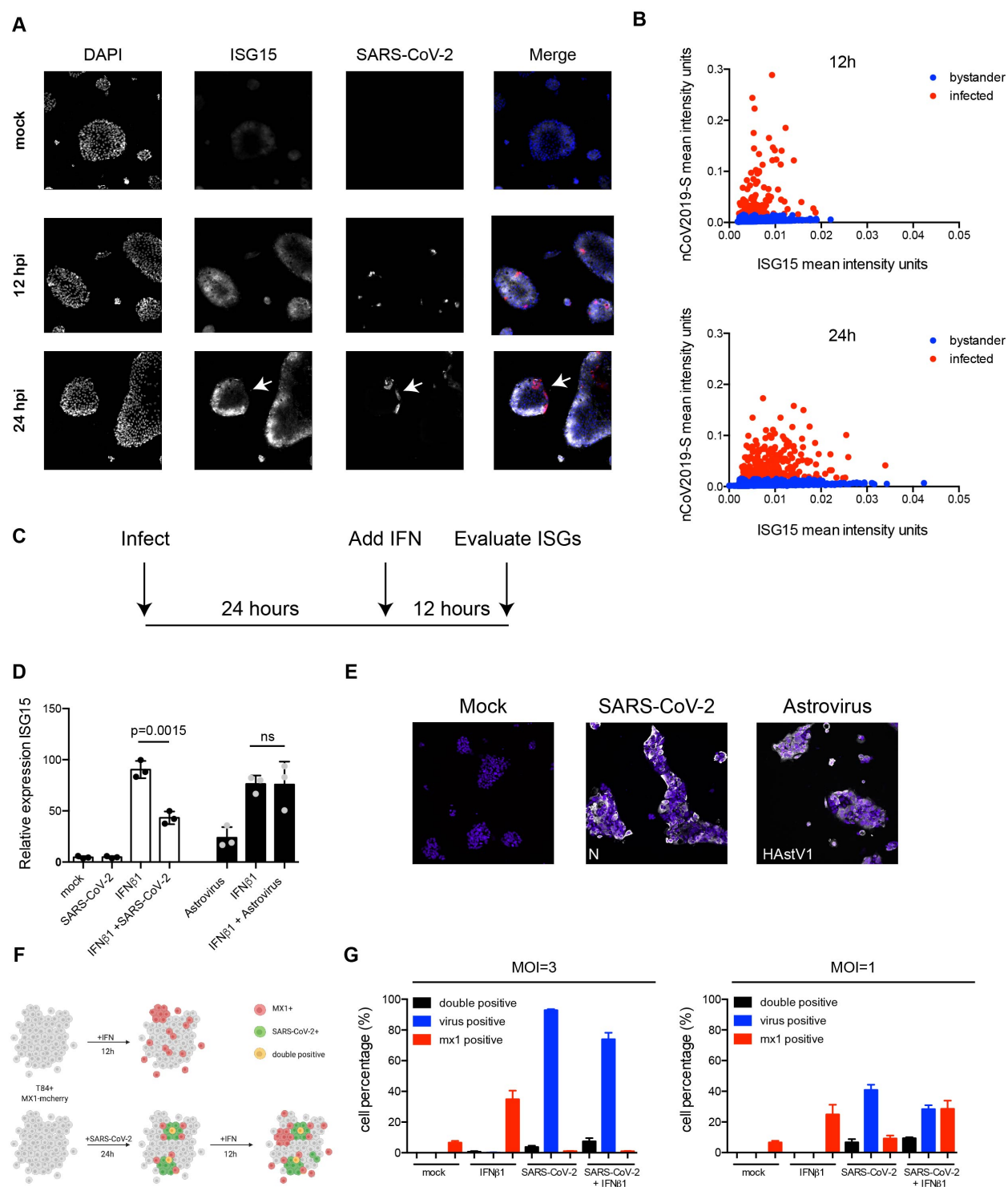
24

686

Figure 6

25

687 **Figure 6.** SARS-CoV-2 infection impairs interferon-mediated signaling. A. Human ileum-derived
688 organoids were seeded in 2D on iBIDi chamber slides. 12 and 24 hpi cells were fixed and the
689 amount of SARS-CoV-2 infected cells (red) and the induction of ISG15 (white) was analyzed by
690 single molecule RNA FISH. Nuclei were visualized with DAPI (blue). Representative image is
691 shown. B. Quantification of the mean fluorescence intensity of samples in A. Each dot represents
692 a cell. C. Schematic depicting the infection and interferon addition to evaluate ISG15 induction
693 following SARS-CoV-2 and astrovirus infection. D. T84 IRF3 knock-out cells were infected with
694 SARS-CoV-2 or human astrovirus 1 at an MOI=3. 24 hpi, cells were incubated in the presence or
695 absence of 2000 IU/mL of IFNβ1. 12 h post-treatment RNA was harvested and the induction of
696 ISG15 was analyzed by q-RT-PCR. Three biological replicates were performed. Error bar
697 indicates standard deviation. Statistics were determined by unpaired t-test. E. T84 IRF3 knock-
698 out cells were infected with SARS-CoV-2 or human astrovirus 1 at an MOI=3. 24 hpi, cells were
699 fixed and stained for either the SARS-CoV-2 N protein or for human astrovirus 1 (HAstV1) capsid
700 protein. Experiments were performed in triplicate. Representative image is shown. F. Schematic
701 depicting the T84 MX-1 mcherry expressing cells and their response to IFN or SARS-CoV-2
702 infection. G. T84 MX-1 mcherry were infected with SARS-CoV-2 at an MOI=3 or MOI=1. 24 hpi
703 cells were incubated in the presence or absence of 2000 IU/mL of IFNβ1. 12 h post-treatment
704 cells were fixed and stained for SARS-CoV-2 N protein. The number of MX-1 positive, SARS-
705 CoV-2 positive and double positive cells was quantified. Three biological replicates were
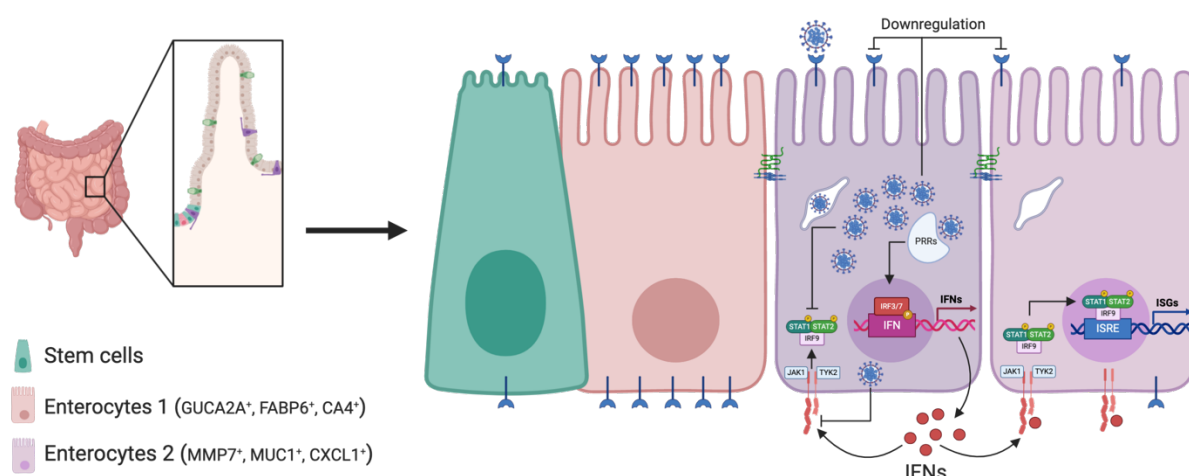706 performed. Error bar indicates standard deviation.
707

Figure 7. Schematic of SARS-CoV-2 infection of human intestinal epithelial cells. SARS-CoV-2 infects a subpopulation of enterocytes. Upon infection, enterocytes mount a pro-inflammatory response characterized by the upregulation of NFκB and TNF. Bystander cells respond to secreted IFN and upregulate the expression of ISGs. SARS-CoV-2 infection induces the downregulation of ACE2 expression and interferes with IFN-mediated signalling in infected cells.

716

Methods

718

Cells

720 T84 human colon carcinoma cells (ATCC CCL-248) and their knock-out derivative clones were
721 maintained in a 50:50 mixture of Dulbecco's modified Eagle's medium (DMEM) and F12 (GibCo)
722 supplemented with 10% fetal bovine serum and 1% penicillin/streptomycin (Gibco). Vero E6
723 (ATCC CRL 1586) were maintained in DMEM supplemented with 10% fetal bovine serum and
724 1% penicillin/streptomycin. The mCherry-tagged Mx1 promoter plasmid was a kind gift from
725 Ronald Dijkman (University of Bern), which was used to generate a T84 stable cell line via
726 lentiviral transduction. Single clones were derived from this cell line and evaluated for their ability
727 to respond to both type-I and type-III interferons.

728

Viruses

730 SARS-CoV-2 (strain BavPat1) was obtained from the European Virology Archive. The virus was
731 amplified in Vero E6 cells.

732

Human organoid cultures and ethic approval

734 Human tissue was received from colon resection or ileum biopsies from the University Hospital
735 Heidelberg. This study was carried out in accordance with the recommendations of the University
736 Hospital Heidelberg with informed written consent from all subjects in accordance with the
737 Declaration of Helsinki. All samples were received and maintained in an anonymized manner.
738 The protocol was approved by the "Ethics commission of the University Hospital Heidelberg"
739 under the protocol S-443/2017. Organoids were prepared following the original protocol described
740 by [46]. In brief, stem cells containing crypts were isolated following 2 mM EDTA dissociation of
741 tissue samples for 1 h at 4°C. Crypts were spun and washed in ice cold PBS. Fractions enriched
742 in crypts were filtered with 70 mM filters and the fractions were observed under a light microscope.
743 Fractions containing the highest number of crypts were pooled and spun again. The supernatant
744 was removed, and crypts were re-suspended in Matrigel. Crypts were passaged and maintained
745 in basal and differentiation culture media as previously described [43].

746

2D organoid seeding

748 8-well iBIDI glass bottom chambers were coated with 2.5% human collagen in water for 1 h prior
749 to organoids seeding. Organoids were collected at a ratio of 100 organoids/well. Collected
750 organoids were spun at 450 xg for 5 mins and the supernatant was removed. Organoids were
751 washed 1X with cold PBS and spun at 450 xg for 5 mins. PBS was removed and organoids were
752 digested with 0.5% Trypsin-EDTA (Life technologies) for 5 mins at 37°C. Digestion was stopped
753 by addition of serum containing medium. Organoids were spun at 450 xg for 5 mins and the
754 supernatant was removed and organoids were re-suspended in normal growth media at a ratio of
755 250 μL media/well. The collagen mixture was removed from the iBIDI chambers and 250 μL of
756 organoids were added to each well.

757

Viral infections

759 Media was removed from cells and 10^6 pfu of SARS-CoV-2 (as determined in Vero cells) was

760   added to cells for 1 hour at 37°C. Virus was removed, cells were washed 1x with PBS and fresh
761   media was added back to the cells.
762

763   **RNA isolation, cDNA, and qPCR**
764   RNA was harvested from cells using RNAeasy RNA extraction kit (Qiagen) as per manufacturer's
765   instructions. cDNA was made using iSCRIPT reverse transcriptase (BioRad) from 250 ng of total
766   RNA as per manufacturer's instructions. q-PCR was performed using iTaq SYBR green (BioRad)
767   as per manufacturer's instructions, TBP was used as normalizing genes. Primers used:
768

Primer	Sequence (5' to 3')
TBP forward	CCACTCACAGACTCTCACAAC
TBP reverse	CTGCGGTACAATCCCAGAACT
IFNb1 forward	GCCGCATTGACCATCTAT
IFNb1 reverse	GTCTCATTCCAGCCAGTG
IFNL1 forward	GCAGGTTCAAATCTCTGTCAC
IFNL1 reverse	AAGACAGGAGAGCTGCAACTC
IFNL2/3 forward	GCCACATAGCCCAGTTCAAG
IFNL2/3 reverse	TGGGAGAGGATATGGTGCAG
CoV2 forward	GCCTCTTCTCGTTCC
CoV2 reverse	AGCAGCATCACCGCC
ISG15 forward	CCTCTGAGCATCCTGGT
ISG15 reverse	AGGCCGTACTCCCCCAG
IFIT1 forward	AAAAGCCCACATTTGAGGTG

IFIT1 reverse	GAAATTCCTGAAACCGACCA

769

Indirect immunofluorescence assay

T84 cells were seeded on iBIDI glass bottom 8-well chamber slides 24 h prior to infection. At indicated times post-infection, cells were fixed in 4% paraformaldehyde (PFA) for 20 mins at room temperature (RT). Cells were washed and permeabilized in 0.5% Triton-X for 15 mins at RT. Mouse monoclonal antibody against SARS-CoV NP (Sino biologicals MM05) and mouse monoclonal against J2 (scions) were diluted in phosphate-buffered saline (PBS) at 1/1000 dilution and incubated for 1h at RT. Cells were washed in 1X PBS three times and incubated with secondary antibodies (conjugated with AF488 (Molecular Probes), or AF568 (Molecular Probes) directed against the animal source) and DAPI for 45 mins at RT. Cells were washed in 1X PBS three times and maintained in PBS. Cells were imaged by epifluorescence on a Nikon Eclipse Ti-S (Nikon).

In-cell western

20,000 Vero E6 cells were seeded per well into a 96-well dish 24 hours prior to infection. 100μL of harvested supernatant was added to the first well. Seven serial 1:10 dilutions were made (all samples were performed in triplicate). Infections were allowed to proceed for 24h. 24 hours post-infection cells were fixed in 2% PFA for 20 mins at RT. PFA was removed and cells were washed twice in 1X PBS and then permeabilized for 10 mins at RT in 0.5% Triton-X. Cells were blocked in a 1:2 dilution of Li-Cor blocking buffer (Li-Cor) for 30 mins at RT. Cells were stained with 1/1000 dilution anti-dsRNA (J2) for 1 h at RT. Cells were washed three times with 0.1% Tween in PBS. Secondary antibody (anti-mouse CW800) and DNA dye Draq5 (Abcam) were diluted 1/10,000 in blocking buffer and incubated for 1 h at RT. Cells were washed three times with 0.1% Tween/PBS. Cells were imaged in 1X PBS on a LICOR imager.

Organoid dissociation for scRNAseq

2D seeded organoids harvested after 0 (mock), 12 and 24 hours post-infection were washed in cold PBS and incubated in TrypLE Express (Gibco) for 25 min at 37°C. When microscopic examination revealed that cells had reached a single cell state, they were resuspended in DMEM/F12 and spun at 500 xg for 5 mins. Supernatant was removed and the cell pellet was resuspended in PBS supplemented with 0.04% BSA and passed through a 40 μm cell strainer. Resulting cell suspensions were used directly for single-cell RNAseq.

Single-cell RNA-seq library preparation

Single-cell suspensions were loaded onto the 10x Chromium controller using the 10x Genomics Single Cell 3' Library Kit NextGem (10x Genomics) according to the manufacturer's instructions. In summary, cell and bead emulsions were generated, followed by reverse transcription, cDNA amplification (5 μL of of amplified cDNA was set apart for targeted scRNAseq amplification), fragmentation, and ligation with adaptors followed by sample index PCR. Resulting libraries were quality checked by Qubit and Bioanalyzer, pooled and sequenced using HiSeq4000 (Illumina; high-output mode, paired-end 26 x 75 bp).

810

Targeted single-cell RNA-sequencing

For targeted scRNAseq, outer and inner primers for targeted amplification were designed using an R package for primer design described in [24] and available through Bioconductor (http://bioconductor.org/packages/release/bioc/html/TAPseq.html). Primers were ordered desalted as ssDNA oligonucleotides and pooled in an equimolar amount, except for the primer targeting SARS-CoV-2 mRNA which was added in 8-fold excess to the outer and inner panel. All primer sequences are described in Supplementary Table 1. Targeted scRNA-seq was performed as previously described [24], except for using amplified cDNA from the 10X Genomics 3' scRNA-seq protocol as input material. In short, 10 ng of amplified cDNA were used as input for the outer primer PCR and amplified with 10 PCR cycles. A second seminested PCR using 10 ng of Ampure purified outer PCR as input was performed with inner primer mix and 7 cycles of PCR. Then, a third PCR was done adding Illumina adapters. Resulting libraries were quality checked by Qubit and Bioanalyzer, pooled and sequenced using HiSeq4000 (Illumina; high-output mode, paired-end 26 x 75 bp).

Pre-processing and quality control of scRNAseq data

Raw sequencing data was processed using the CellRanger software (version 3.1.0). Reads were aligned to a custom reference genome created with the reference human genome (GRCh38) and SARS-CoV-2 reference genome (NC_045512.2). The resulting unique molecular identifier (UMI) count matrices were imported into R (version 3.6.2) and processed with the R package Seurat (version 3.1.3). Low-quality cells were removed, based on the following criteria. All cells with mitochondrial reads > 30% were excluded. Second, we limited the acceptable numbers of detected genes. For both types of samples, cells with <1500 or >9000 detected genes were discarded. The remaining data were further processed using Seurat. To account for differences in sequencing depth across cells, UMI counts were normalized and scaled using regularized negative binomial regression as part of the package sctransform. Afterward, ileum and colon organoids samples were integrated independently to minimize the batch and experimental variability effect. Integration was performed using the canonical correlation analysis and mutual nearest neighbor analysis. The resulting corrected counts were used for visualization and clustering downstream analysis and non-integrated counts for any quantitative comparison.

Pre-processing of targeted scRNAseq

Targeted scRNA-seq pre-processing was done as described in [24]. In summary, following demultiplexing by sample, sequencing data were processed following the workflow provided by Drop-seq tools (v. 1.13, http://mccarrolllab.org/dropseq/) with STAR (v. 2.5.3a) to align reads. To mitigate potential multi-mapping issues, targeted samples were aligned to a custom alignment reference containing only genes of the respective target gene panel, including the SARS-CoV-2 genome. This reference contained the sequences of all target gene loci as individual contigs with overlapping loci merged into one contig. UMI observations were extracted using the Drop-seq tools GatherMolecularBarcodeDistributionByGene program. A custom script (Python v. 3.6.6) was used to filter for chimeric reads with a transcripts-per-transcript (TPT) cutoff of 0.25, and UMI observations were converted to transcript counts. Cell-containing droplets were extracted using the filtered cell barcodes from the scRNASeq data. Other detected cell barcodes droplets were categorized as empty droplets. The infection status for every cell was extracted from the targeted

855   gene expression data by thresholding the SARS-CoV-2 counts using the media expression of the
856   cell containing droplets (Figure S2). Furthermore, Pearson correlation of each targeted gene to
857   its WTA equivalent was calculated.
858

859   **Clustering and identification of cell type markers**
860   We performed principal component analysis (PCA) using 3000 highly variable genes (based on
861   average expression and dispersion for each gene). The top 30 principal components were used
862   to construct a shared nearest neighbor (SNN) graph and modularity-based clustering using the
863   Louvain algorithm was performed. Finally, Uniform manifold approximation and projection
864   (UMAP) visualization was calculated using 30 neighboring points for the local approximation of
865   the manifold structure. Marker genes for every cell type were identified by comparing the
866   expression of each gene in a given cluster against the rest of the cells using the receiver operating
867   characteristic (ROC) test. To evaluate which genes classify a cell type, the markers were selected
868   as those with the highest classification power defined by the AUC (area under the ROC curve).
869   These markers along with canonical markers for intestinal and colonic cells were used to annotate
870   each of the clusters of the ileum and colon samples.
871

872   **Differential expression analysis**
873   To identify the changes in expression across conditions. Differential expression tests were
874   performed using MAST [47]. To reduce the size of the inference problem and avoid cell proportion
875   bias, separate models were fit for each cell lineage and comparisons between mock, 12 hours,
876   and 24 hours post-infection were performed. False discovery rate (FDR) was calculated by the
877   Benjamini-Hochberg method [48] and significant genes were set as those with FDR of less than
878   0.05. Subsequently, genes whose mRNAs were found to be differentially expressed were
879   subjected to a gene set overrepresentation analysis using the EnrichR package in R. Furthermore
880   signalling pathways enrichment was calculated using PROGENy.
881

882   **Multiplex FISH**
883   Organoids were seeded in expansion medium on glass coverslips. At 24 hours post-seeding, the
884   expansion medium was replaced by differentiation medium and organoids were left to differentiate
885   for 4 days. After validation that organoids were differentiated and contained all expected cell
886   types, organoids were infected, harvested after 12 and 24 hpi, and fixed in 4% PFA for 30 minutes.
887   HiPlex (RNAscope) was performed following the manufacturer's instructions. Briefly, fixed
888   samples were dehydrated with 50%, 70%, 100% ethanol, then treated with protease. All the
889   HiPlex probes were hybridized and amplified together. Probes were designed for genes identified
890   as cell type markers and/or corroborated by literature. The probes used were:
891

Gene name	Role of the marker	Catalog number
ACE2	SARS-CoV-22 Receptor	848151
ISG15	Infection Marker	311021
nCoV2019-S	SARS-CoV-22 marker	848561

892

893 After washing, cell nuclei were counterstained with DAPI, and samples were mounted using
894 ProLong Gold Antifade Mountant. Imaging was performed with the camera Nikon DS-Qi2 (Nikon
895 Instruments) with the Plan Fluor 20x objective (Nikon Instruments) mounted on the Nikon Ti-E
896 inverted microscope (Nikon Instruments) in bright-field and fluorescence (DAPI, GFP, Cy3 and
897 Cy5 channels). The microscope was controlled using the Nikon NIS Elements software. After
898 each round, fluorophores were cleaved and samples moved on to the next round of the
899 fluorophore detection procedures. All images from all rounds of staining were then registered with
900 each other to generate images using HiPlex image registration software (ACD Bio). Further
901 brightness and contrast adjustments were performed using Fiji.
902
903 The HiPlex probe fluorescent signal was used to determine the ACE2 and ISG15 RNA expression
904 levels, as well as the SARS-CoV-2 infection levels. To obtain a resolution at a single cell level,
905 first nuclei segmentation and classification was done on raw DAPI images using the Pixel
906 Classification + Object Classification workflow from ilastik 1.2.0. The resulting Object Prediction
907 masks represented all nuclei as individual objects in a 2D plane and were saved as 16bit Tagged
908 Image File Format. To measure the single cell fluorescent intensity for the ACE2, ISG15 and
909 SARS-CoV-2 probes, a pipeline using CellProfiler 3.1.9 was developed. Briefly, first the raw
910 grayscale images corresponding to the ACE2, ISG15 and SARS-CoV-2 probe fluorescent signals
911 were uploaded on the pipeline. These images were specified as images to be measured. The
912 corresponding Object Prediction masks previously generated by ilastik were then uploaded,
913 converted into binary nuclei masks and used to define the objects to be measured. Finally, with a
914 MeasureObjectIntesity module the fluorescence intensity features, the cell number and the single
915 cell localization were measured for the identified objects from the binary nuclei mask. The
916 outcome was exported to a spreadsheet and contained the localization as well as the mean
917 intensity units rescaled from 0 to 1 of ACE2, ISG15 and SARS-CoV-2 fluorescent signals for each
918 single cell.
919
920 To determine the infection status for every cell a threshold was calculated using the SARS-CoV-
921 2 mean fluorescent intensity signal of mock treated versus representative infected cells. The
922 threshold was set to 0.015 mean intensity units. Due to the probe quality, the ACE2 fluorescent
923 signal showed strong variations between different images and hence technical replicates. To
924 minimize the variability, for each individual image the ACE2 mean intensity signal was normalized
925 and rescaled from 0 to 1, 0 corresponding to the lowest and 1 to the highest ACE2 mean intensity
926 signal of a cell from the corresponding image. Finally, the SARS-CoV2 mean intensity signal was
927 plotted against the normalized ACE mean intensity signal or the ISG15 mean intensity signal
928 using GraphPad Prism Version 6.0.
929
930 **Transcription factor activity along diffusion map pseudotime**
931 Raw counts were normalised using the SCTransform method implemented in Seurat v. 3.2.0,
932 regressed out over UMI counts. Transcription factor activities were then calculated using
933 pySCENIC v 0.10.13 (Sande et al. 2020). Independently, the diffusion maps were computed using
934 the destiny R library v 3.2.0. For the inference of pseudotime in Ileum a set of curated genes
935 related to IFN signaling from Reactome were used as input. For colon, we also added genes with
936 highest variability (standard deviation > 2). Visualisation of the TF activities along trajectories were

937   carried out with custom R scripts (v 4.0.2).

938

939   **Data and Code Availability**

940   The raw sequencing generated during this study is available at the NCBI Gene Expression
941   Omnibus (accession no. GSE156760). The authors declare that all other data supporting the
942   findings of this study are within the manuscript and its supplementary files.
943

References

944

945 1   Giamarellos-Bourboulis EJ, Netea MG, Rovina N, *et al.* Complex Immune Dysregulation in
946   COVID-19 Patients with Severe Respiratory Failure. *Cell Host Microbe* 2020;**27**:992–
947   1000.e3.

948 2   Zhou Z, Ren L, Zhang L, *et al.* Heightened Innate Immune Responses in the Respiratory
949   Tract of COVID-19 Patients. *Cell Host Microbe* 2020;**27**:883–90.e2.

950 3   Mehta P, McAuley DF, Brown M, *et al.* COVID-19: consider cytokine storm syndromes and
951   immunosuppression. *Lancet* 2020;**395**:1033–4.

952 4   Chen G, Wu D, Guo W, *et al.* Clinical and immunological features of severe and moderate
953   coronavirus disease 2019. *J Clin Invest* 2020;**130**:2620–9.

954 5   Mathew D, Giles JR, Baxter AE, *et al.* Deep immune profiling of COVID-19 patients reveals
955   patient heterogeneity and distinct immunotypes with implications for therapeutic
956   interventions. *bioRxiv* Published Online First: 23 May 2020.
957   doi:10.1101/2020.05.20.106401

958 6   Lucas C, Wong P, Klein J, *et al.* Longitudinal analyses reveal immunological misfiring in
959   severe COVID-19. *Nature* Published Online First: 27 July 2020. doi:10.1038/s41586-020-
960   2588-y

961 7   Hoffmann M, Kleine-Weber H, Schroeder S, *et al.* SARS-CoV-2 Cell Entry Depends on
962   ACE2 and TMPRSS2 and Is Blocked by a Clinically Proven Protease Inhibitor. *Cell*
963   2020;**181**:271–80.e8.

964 8   Bestle D, Heindl MR, Limburg H, *et al.* TMPRSS2 and furin are both essential for proteolytic
965   activation of SARS-CoV-2 in human airway cells. *Life Sci Alliance* 2020;**3**.
966   doi:10.26508/lsa.202000786

967 9   Stanifer ML, Pervolaraki K, Boulant S. Differential Regulation of Type I and Type III
968   Interferon Signaling. *Int J Mol Sci* 2019;**20**. doi:10.3390/ijms20061445

969 10 Prasad A, Prasad M. Single Virus Targeting Multiple Organs: What We Know and Where
970   We Are Heading? *Front Med* 2020;**7**:370.

971 11 Gupta A, Madhavan MV, Sehgal K, *et al.* Extrapulmonary manifestations of COVID-19. *Nat*
972   *Med* Published Online First: 10 July 2020. doi:10.1038/s41591-020-0968-3

973 12 Wu Y, Guo C, Tang L, *et al.* Prolonged presence of SARS-CoV-2 viral RNA in faecal
974   samples. *Lancet Gastroenterol Hepatol* 2020;**5**:434–5.

975 13 Xiao F, Tang M, Zheng X, *et al.* Evidence for Gastrointestinal Infection of SARS-CoV-2.
976   Gastroenterology. 2020;**158**:1831–3.e3.

977 14 Xing Y-H, Ni W, Wu Q, *et al.* Prolonged viral shedding in feces of pediatric patients with
978   coronavirus disease 2019. *J Microbiol Immunol Infect* 2020;**53**:473–80.

979 15 Wölfel R, Corman VM, Guggemos W, *et al.* Virological assessment of hospitalized patients
980   with COVID-2019. *Nature* 2020;**581**:465–9.

16   Lamers MM, Beumer J, van der Vaart J, *et al.* SARS-CoV-2 productively infects human gut enterocytes. *Science* Published Online First: 1 May 2020. doi:10.1126/science.abc1669

17   Stanifer ML, Kee C, Cortese M, *et al.* Critical Role of Type III Interferon in Controlling SARS-CoV-2 Infection in Human Intestinal Epithelial Cells. *Cell Rep* 2020;**32**:107863.

18   Zang R, Gomez Castro MF, McCune BT, *et al.* TMPRSS2 and TMPRSS4 promote SARS-CoV-2 infection of human small intestinal enterocytes. *Sci Immunol* 2020;**5**. doi:10.1126/sciimmunol.abc3582

19   Blanco-Melo D, Nilsson-Payant BE, Liu W-C, *et al.* Imbalanced Host Response to SARS-CoV-2 Drives Development of COVID-19. *Cell* 2020;**181**:1036–45.e9.

20   Hadjadj J, Yatim N, Barnabei L, *et al.* Impaired type I interferon activity and inflammatory responses in severe COVID-19 patients. *Science* Published Online First: 13 July 2020. doi:10.1126/science.abc6027

21   Zhou J, Li C, Liu X, *et al.* Infection of bat and human intestinal organoids by SARS-CoV-2. *Nat Med* 2020;**26**:1077–83.

22   Smillie CS, Biton M, Ordovas-Montanes J, *et al.* Intra- and Inter-cellular Rewiring of the Human Colon during Ulcerative Colitis. *Cell* 2019;**178**:714–30.e22.

23   Triana S, Stanifer ML, Shahraz M, *et al.* Single-cell transcriptomics reveals immune response of intestinal cell types to viral infection. 2020;:2020.08.19.255893. doi:10.1101/2020.08.19.255893

24   Schraivogel D, Gschwind AR, Milbank JH, *et al.* Targeted Perturb-seq enables genome-scale genetic screens in single cells. *Nat Methods* 2020;**17**:629–35.

25   Ziegler CGK, Allon SJ, Nyquist SK, *et al.* SARS-CoV-2 Receptor ACE2 Is an Interferon-Stimulated Gene in Human Airway Epithelial Cells and Is Detected in Specific Cell Subsets across Tissues. *Cell* 2020;**181**:1016–35.e19.

26   Chua RL, Lukassen S, Trump S, *et al.* COVID-19 severity correlates with airway epithelium-immune cell interactions identified by single-cell analysis. *Nat Biotechnol* Published Online First: 26 June 2020. doi:10.1038/s41587-020-0602-4

27   Froggatt HM, Harding AT, Heaton NS. ETV7 represses a subset of interferon-stimulated genes that restrict influenza viruses. 2019;:851543. doi:10.1101/851543

28   Zhu Z, Du X, Li P, *et al.* Early Growth Response Gene-1 Suppresses Foot-and-Mouth Disease Virus Replication by Enhancing Type I Interferon Pathway Signal Transduction. *Front Microbiol* 2018;**9**:2326.

29   Wyler E, Kirstin M, Vedran F, *et al.* Bulk and single-cell gene expression profiling of SARS-CoV-2 infected human cell lines identifies molecular targets for therapeutic intervention. bioRxiv. 2020;:2020.05.05.079194. doi:10.1101/2020.05.05.079194

30   Qi F, Qian S, Zhang S, *et al.* Single cell RNA sequencing of 13 human tissues identify cell types and receptors of human coronaviruses. *Biochem Biophys Res Commun* 2020;**526**:135–40.

31   Ravindra NG, Alfajaro MM, Gasque V, *et al.* Single-cell longitudinal analysis of SARS-CoV-2 infection in human bronchial epithelial cells. *bioRxiv* Published Online First: 7 May 2020. doi:10.1101/2020.05.06.081695

32   Han L, Wei X, Liu C, *et al.* Single-cell atlas of a non-human primate reveals new pathogenic mechanisms of COVID-19. 2020;:2020.04.10.022103. doi:10.1101/2020.04.10.022103

33   Zhou L, Niu Z, Jiang X, *et al.* Systemic analysis of tissue cells potentially vulnerable to SARS-CoV-2 infection by the protein-proofed single-cell RNA profiling of ACE2, TMPRSS2 and Furin proteases. 2020;:2020.04.06.028522. doi:10.1101/2020.04.06.028522

34   Singh M, Bansal V, Feschotte C. A single-cell RNA expression map of human coronavirus entry factors. *Cell Rep*;:108175.

35   Lukassen S, Chua RL, Trefzer T, *et al.* SARS-CoV-2 receptor ACE2 and TMPRSS2 are primarily expressed in bronchial transient secretory cells. *EMBO J* 2020;**39**:e105114.

36   Zhao Y, Zhao Z, Wang Y, *et al.* Single-Cell RNA Expression Profiling of ACE2, the Receptor of SARS-CoV-2. *Am J Respir Crit Care Med* 2020;**202**:756–9.

37   Sungnak W, Huang N, Bécavin C, *et al.* SARS-CoV-2 entry factors are highly expressed in nasal epithelial cells together with innate immune genes. *Nat Med* 2020;**26**:681–7.

38   Onabajo OO, Banday AR, Stanifer ML, *et al.* Interferons and viruses induce a novel truncated ACE2 isoform and not the full-length SARS-CoV-2 receptor. *Nat Genet* Published Online First: 19 October 2020. doi:10.1038/s41588-020-00731-9

39   Neufeldt CJ, Cerikan B, Cortese M, *et al.* SARS-CoV-2 infection induces a pro-inflammatory cytokine response through cGAS-STING and NF-κB. 2020;:2020.07.21.212639. doi:10.1101/2020.07.21.212639

40   Park A, Iwasaki A. Type I and Type III Interferons - Induction, Signaling, Evasion, and Application to Combat COVID-19. *Cell Host Microbe* 2020;**27**:870–8.

41   Stanifer ML, Rippert A, Kazakov A, *et al.* Reovirus intermediate subviral particles constitute a strategy to infect intestinal epithelial cells by exploiting TGF-β dependent pro-survival signaling. *Cell Microbiol* 2016;**18**:1831–45.

42   Pervolaraki K, Stanifer ML, Münchau S, *et al.* Type I and Type III Interferons Display Different Dependency on Mitogen-Activated Protein Kinases to Mount an Antiviral State in the Human Gut. *Front Immunol* 2017;**8**:459.

43   Stanifer ML, Mukenhirn M, Muenchau S, *et al.* Asymmetric distribution of TLR3 leads to a polarized immune response in human intestinal epithelial cells. *Nat Microbiol* 2020;**5**:181–91.

44   Kayisoglu O, Weiss F, Niklas C, *et al.* Location-specific cell identity rather than exposure to GI microbiota defines many innate immune signalling cascades in the gut epithelium. *Gut* Published Online First: 22 June 2020. doi:10.1136/gutjnl-2019-319919

45   Lei X, Dong X, Ma R, *et al.* Activation and evasion of type I interferon responses by SARS-CoV-2. *Nat Commun* 2020;**11**:3810.

1057 46 Sato T, Stange DE, Ferrante M, *et al.* Long-term expansion of epithelial organoids from
1058 human colon, adenoma, adenocarcinoma, and Barrett's epithelium. *Gastroenterology*
1059 2011;**141**:1762–72.

1060 47 Finak G, McDavid A, Yajima M, *et al.* MAST: a flexible statistical framework for assessing
1061 transcriptional changes and characterizing heterogeneity in single-cell RNA sequencing
1062 data. Genome Biology. 2015;**16**. doi:10.1186/s13059-015-0844-5

1063 48 Benjamini Y, Hochberg Y. Controlling the False Discovery Rate: A Practical and Powerful
1064 Approach to Multiple Testing. Journal of the Royal Statistical Society: Series B
1065 (Methodological). 1995;**57**:289–300. doi:10.1111/j.2517-6161.1995.tb02031.x

1066